MASTER THESIS

By

Verónica COLLADO CIPRÉS

Nano-structured vanadium oxide thin films for gas sensors

Thesis submitted for the degree of Master of Science in Industrial Engineering, specialization materials.

Tutor:
Nicolas MARTIN, Professor, École Nationale Supérieure de Mécanique et des Microtechniques (ENSMM)

Academic year 2013-2014

Acknowledgements

"Hoy es siempre todavía"- Antonio Machado

After six months of intriguing work, my master thesis has come to an end. This means I have concluded my Master Degree, being able to call myself Engineer. During these months, I had a revelation: discovering the world of research, notably in materials science. This work has given me the great satisfaction of loving what I did and enjoying the challenges and successes like never before. It has opened many doors in my mind and rang bells I did not even know existed till now.

I have plenty of people to thank for this experience. Firstly, ENSMM and the research institute FEMTO-ST for offering me the opportunity of doing my master thesis with them in collaboration with my university ETSEIB. Most specially, I would like to thank my tutor, Prof. Nicolas Martin, who offered me this Master thesis subject. Prof. Nicolas Martin can be described as the most committed, brilliant and kind-hearted tutor and person. His priceless help throughout the thesis let me pursue higher goals whilst feeling the hard work recognised. I have tried to learn as much as I could, both academically and personally, from him and I am certain that we will work together for other projects in the future. Further, I would like to thank Prof. Gonzalo Cabodevila for his help in the thesis subject hunt for Spanish students like me, Jean-Yves Rauch and Jean-Baptiste Sanchez for their selfless work helping me and all my colleges from the FEMTO-ST MN2S department for their interest and kindness. I cannot forget to thank Marta Horakova for the hours spent together in the lab, her great sense of humour and expertise advices for my work.

Finally, I would like to enthusiastically thank my family and my boyfriend for all their support during this stay, enjoying of the happiness I have experienced as if it were their own. Also, huge thanks to all the fabulous friends I have met in Besançon and to my good friend Edgard Vilaseca, who has been next to me since first degree and without whom nothing would have been the same.

Thank you all!
Moltes gràcies a tots!
¡Gracias a todos!
Merci à tous!

Verónica Collado Ciprés

Contents

Abstract

Vanadium thin films are prepared by DC magnetron sputtering using the GLancing Angle Deposition (GLAD) method. This technique will allow the growth of porous nano-structures with inclined columns, as well as zig-zags and spirals. Also pulses of oxygen combined with GLAD will be used during sputtering to study the properties of the films. All films are oxidized after being heated for several temperature cycles, taking the forms of V_2O_5 and VO_X compositions. The aim of this work is to characterize coatings containing primarily the VO_2 phase; given this phase has a reversible semi-conductor to metal transition close to room temperature (Approximately 68º). Due to this behaviour, VO_2 becomes useful in sensor applications, especially with gases. The best operating conditions to favour the formation of VO_2 and its most significant metal-to-semiconductor transition will be examined. The column angle β is measured by scanning electron microscopy (SEM) and the electrical conductivity of the films exhibiting inclined columns, zig-zags and spirals nano-structures as well as the films sputtered with oxygen pulses is investigated with DC-resistivity measurements. It is found that the column angle β must reach a threshold value to significantly reduce the electrical conductivity of the vanadium thin films close to one order of magnitude. The most suitable nano-structures for gas sensor applications found were: Inclined columns of incidence angle $\alpha = 85^0$ annealed to 550ºC and inclined columns of incidence angle $\alpha = 85^0$ with oxygen pulses during deposition with a period of 16 seconds and duty cycles $dc = 0{,}124$ and $dc = 0{,}375$, with annealing treatments to 550ºC and 500ºC respectively. The film with dc=0,375 annealed to 550ºC was tested for ozone sensing. The optimum working temperature found was of 370ºC degrees, with a maximum variation of resistivity in front of time of 0,05534 Ω/s.

List of figures and tables

List of figures

List of tables

List of abbreviations

ALD	Atomic Layer Deposition
CVD	Chemical Vapour Deposition
DC	Direct Current
EBPVD	Electron Beam Physcal Vapour Deposition
GLAD	Glancing Angle Deposition
HIPIMS	High-Power Impulse Magnetron Sputtering
MIT	Metal-to-Insulator Transition
PLD	Pulsed Laser Deposition
PVD	Physical Vapour Deposition
RF	Radio Frequency
RRSP	Reactive Sputtering
SEM	Scanning Electron Microscopy
SIMS	Secondary Ion Mass Spectrometry
TCR	Temperature Coefficient of Resistivity
TFEL	Thin Film Electroluminescent
UV	Ultraviolet
XPS	X-ray Photoelectron Spectroscopy
XRD	X-ray Diffraction

1. Introduction

Concern about the high levels of pollution all around the world causes the regulations towards emissions to become each time stricter. Related to atmospheric gas emissions, innovative gas sensor nano-structures and materials are required to satisfy these new demands and are widely studied by scientists worldwide [1]. Solid state semiconducting gas sensors are one of the most popular research topics in the gas sensing science, since metal-insulator transitions have been investigated for many years [2]. This transition can occur due to variations in parameters such as the chemical composition, stress, electric field, magnetic field and temperature [3, 4]. It corresponds to a transformation of states from an insulator (or semiconductor) to a metallic type of conductivity and reversely [5, 6].

Materials exhibiting this behaviour include binary compounds of transition metal oxides [7] such as SnO_2, TiO_2, WO_3, etc. [1]. Vanadium oxides are considered good new candidates for gas sensors and have already been studied to some extent [2]. Several vanadium pentoxide (V_2O_5) nano-structures have demonstrated sensitivity towards NH_3 [8, 9] and amines [10]. Polycrystalline vanadium oxide thin films have shown sensitivity towards NO [11] and NO_2 [12, 13]. Also, Vanadium dioxide (VO_2) nanowires are being investigated as H_2 sensors by taking advantage of its metal-insulator transition (MIT) [14, 15].

These transitions are accompanied by huge resistivity changes, sometimes even over tens of orders of magnitude [16] and vanadium dioxide is of particular interest because its transition occurs near room temperature. The monoclinic (M1) VO_2 phase has a bandgap of 0.6 eV at 25 °C and converts into metallic rutile (R) VO_2 at 68 °C, resulting in a brusque change in bulk electrical resistivity of 2 to 6 orders of magnitude. The VO_2 MIT is revealed in an abrupt interfacial transition of current across a VO_2 barrier interface forming a tunnel junction. In a first tunnel junction form, a two orders of magnitude rough change in contact resistivity induced by the bulk MIT is shown in VO_2-metal contact nano-structures [17, 18]. The working zone of VO_2 is 5.2eV (25 °C) −5.3eV (90 °C). The

brusque change in current across the VO_2 interface is due to the change in free carriers in bulk VO_2 across the MIT [19].

There are several methods for fabricating vanadium oxide thin films, e.g. Chemical vapour deposition [20], sol–gel method [21], pulsed laser deposition (PLD) [22-24], and sputtering methods [25, 26] with posterior annealing. The advantages of sputtering processes are film homogeneity, expandability to larger substrate sizes and efficiency of deposition when compared to the other methods [27].

Thin films with high transition resistivity ratios can be deposited at low temperatures by DC sputtering from a vanadium target in an Argon (Ar) working gas atmosphere using a planar magnetron source. This method enables depositing large surfaces area and a good temperature control [28].

The purpose of this paper is to investigate the electrical conductivity of vanadium oxide thin films exhibiting different nano-structures: Inclined columns, zig-zags and spirals. The operating conditions required for favouring the highest change of electrical resistivity and, therefore, the most significant metal – semiconductor transition are examined. DC magnetron sputtering deposition, implementing the GLancing Angle Deposition (GLAD) method [29, 30] is employed, followed by oxidation by annealing the films in a homemade device. Also, reactive sputtering (RRSP) using oxygen during GLAD is employed in some of the films. The interest will be then to correlate and understand the possible relationships between the structural characteristics, optical and electronic behaviours of the films and their performance as gas sensors.

Bibliography of chapter 1

[1] Huotari J, Lappalainen J, Puustinen J and Lloyd Spetz A 2013 Gas sensing properties of pulsed laser deposited vanadium oxide thin films with various crystal nano-structures *Sensors and Actuators B: Chemical* **187** 386-394.

[2] Fujioka J, Miyasaka S and Tokura Y 2005 Orbital disordering and the metal-insulator transition with hole doping in perovskite-type vanadium oxides *Physical Review B* **72(2)** 024460.

[3] Imada M, Fujimori A and Tokura Y 1998 Metal-insulator transitions *Reviews of Modern Physics* **70(4)** 1039.

[4] Zhou C, Newns D M, Misewich J A and Pattnaik P C 1997 A field effect transistor based on the Mott transition in a molecular layer *Applied physics letters* **70(5)** 598-600.

[5] Chudnovskiy F, Luryi S and Spiva B 2002 Switching device based on a first-order metal-insulator transition induced by an external electric field *Future Trends in Microelectronics: the Nano Millennium* Ed. Luriy S, Xu JM, Zaslavsky A (Part II: The Future Beyond Silicon), New York: John Wiley and Sons Ltd 148-155.

[6] Martens K, Radu I P Mertens S Shi X Nyns L Cosemans S and Jurczak M 2012 The VO2 interface, the metal-insulator transition tunnel junction, and the metal-insulator transition switch On-Off resistance *Journal of Applied Physics* **112(12)** 124501

[7] Besnard A, Martin N, Sthal F, Carpentier L and Rauch J-Y 2013 Metal-to-Dielectric transition induced by annealing of oriented titanium thin films *Functional Materials Letters* **6(01).**

[8] Modaferri V, Panzera G, Donato A, Antonucci P L, Cannilla C, Donato N, Spadaro D and Neri G 2012 Highly sensitive ammonia resistive sensor based on electro-spun V_2O_5 fibers *Sensors and Actuators B* **163** 61–68.

[9] Rizzo G, Arena A, Bonavita A, Donato N, Neri G and Saitta G 2010 Gasochromic response of nanocrystalline vanadium pentoxide films deposited from ethanol dispersions *Thin Solid Films* **518(23)** 7124-7127.

[10] Raible I, Burghard M, Schlecht U, Yasuda A and Vossmeyer T 2005 V_2O_5 nanofibres: novel gas sensors with extremely high sensitivity and selectivity to amines *Sensors and Actuators B: Chemical* **106(2)** 730-735.

[11] Capone S, Rella R, Siciliano P and Vasanelli L 1999 A comparison between V_2O_5 and WO_3 thin films as sensitive elements for NO detection *Thin Solid Films* **350(1)** 264-268.

[12] Rella R, Siciliano P, Cricenti A, Generosi R, Girasole M, Vanzetti L, Anderle M and Coluzza C 1999 A study of physical properties and gas-surface interaction of vanadium oxide thin films *Thin Solid Films* **349** 254–259.

[13] Manno D, Serra A, Di Giulio M, Micocci G, Taurino A, Tepore A and Berti D 1997 Structural and electrical properties of sputtered vanadium oxide thin films for applications as gas sensing material *Journal of Applied Physics* **81** 2709–2714.

[14] Byon J W, Kim M B, Kim M H, Kim S Y, Lee S H, Lee B C and Baik J M 2012 Electrochemically induced highly responsive and highly selective vanadium oxide hydrogen sensor based on metal–insulator transition *Journal of Physical Chemistry C* **116** 226–230.

[15] Baik J M, Kim M H, Larson C, Yavuz C T, Stucky G D, Wodtke A M and Moskovits M 2009 Pd-sensitized single vanadium oxide nanowires: highly responsive hydrogen sensing based on the metal–insulator transition *Nano Letters* **9** 3980–3984.

[16] Imada M, Fujimori A and Tokura Y 1998 Metal-insulator transitions *Reviews of Modern Physics* **70(4)** 1039.

[17] Morin F 1959 Oxides Which Show a Metal-to-Insulator Transition at the Neel Temperature *Phys.Rev.Lett.* **3** 34.

[18] Rosevear W H and Paul W 1973 Hall effect in VO_2 near the semiconductor-to-Metal Transition *Phys. Rev. B* **7** 2109.

[19] Martens K *et al.* 2012 The VO_2 interface, the metal-insulator transition tunnel junction, and the metal-insulator transition switch On-Off resistance *Journal of Applied Physics* **112(12)** 124501.

[20] Vernardou D, Paterakis P, Drosos H, Spanakis E, Povey I M, Pemble M E, Koudoumas E and Katsarakis N 2011 A study of the electrochemical performance of vanadium oxide thin films grown by atmospheric pressure chemical vapour deposition *Solar Energy Materials and Solar Cells* **95** 2842–2847.

[21] Shi Q, Huang W, Yan J, Zhang Y, Mao M, Zhang Y, Xu Y and Zhang Y 2011 Preparation and phase transition characterization of VO2 thin film on single crystal Si (100) substrate by sol–gel process *Journal of Sol–Gel Science and Technology* **59** 591–597.

[22] Givernaud J, Crunteanu A Orlianges J-C, Pothier A, Champeaux C, Catherinot A and Blondy P 2010 Microwave power limiting devices based on the semiconductor–metal transition in vanadium–dioxide thin films *IEEE Trans-actions on Microwave Theory and Techniques* **58** 2352–2361.

[23] Ramana C V, Smith R J, Hussain O M and Julien C M 2004 On the growth mechanism of pulsed-laser deposited vanadium oxide thin films *Materials Science and Engineering B* **111** 218–225.

[24] Julien C, Haro-Poniatowski E, Camacho-López M A, Escobar-Alarcón L and Jímenez-Jarquín J 1999 Growth of V_2O_5 thin films by pulsed laser deposition and their applications in lithium microbatteries *Materials Science and Engineering B* **65** 170–176.

[25] Gopalakrishnan G and Ramanathan S 2011 Compositional and metal–insulator transi-tion characteristics of sputtered vanadium oxide thin films on yttria-stabilized zirconia *Journal of Materials Science* **46** 5768–5774.

[26] Podraza N J, Gauntt B D, Motyka M A, Dickey E C and Horn M W 2012 Electrical and optical properties of sputtered amorphous vanadium oxide thin films *Journal of Applied Physics* **111** 073522.

[27] Nag J 2011 *The solid-solid phase transition in vanadium dioxide thin films: synthesis, physics and application* (Doctoral dissertation) Nashville, Tennessee 41.

[28] Fuls E N, Hensler D H and Ross A R 2004 Reactively sputtered vanadium dioxide thin films *Applied Physics Letters* **10(7)** 199-201.

[29] Lintymer J, Martin N, Chappé J M, Delobelle P and Takadoum J 2004 Influence of zig-zag micronano-structure on mechanical and electrical properties of chromium multilayered thin films *Surface and Coatings Technology* **180** 26-32.

[30] Robbie K, Sit J C and Brett M J 1998 Advanced techniques for glancing angle deposition *Journal of Vacuum Science & Technology B* **16(3)** 1115-1122.

2. State of the art

2.1 Vanadium, vanadium oxides and applications

Vanadium is a grey coloured, ductile transition metal situated in the fifth column of the periodic table of the elements. Its atomic number is 23 and its electronic configuration is [Ar] $3d^3$ $4s^2$. It is commonly known for its use in steel alloys or in titanium based alloys and for its resistance to acid corrosion (hydrochloric and hydrofluoric mostly). It is actually being studied in a new type of batteries called *flow batteries*, which recharge faster than standard batteries [1].

Vanadium is also studied for applications in the nuclear industry to reduce the fuel in the reactor because of its weak capturing neutrons efficient section. In addition, it's been used as dopant in zirconia matrix due to its blue colour [2]. However, it is mostly employed in its oxides forms.

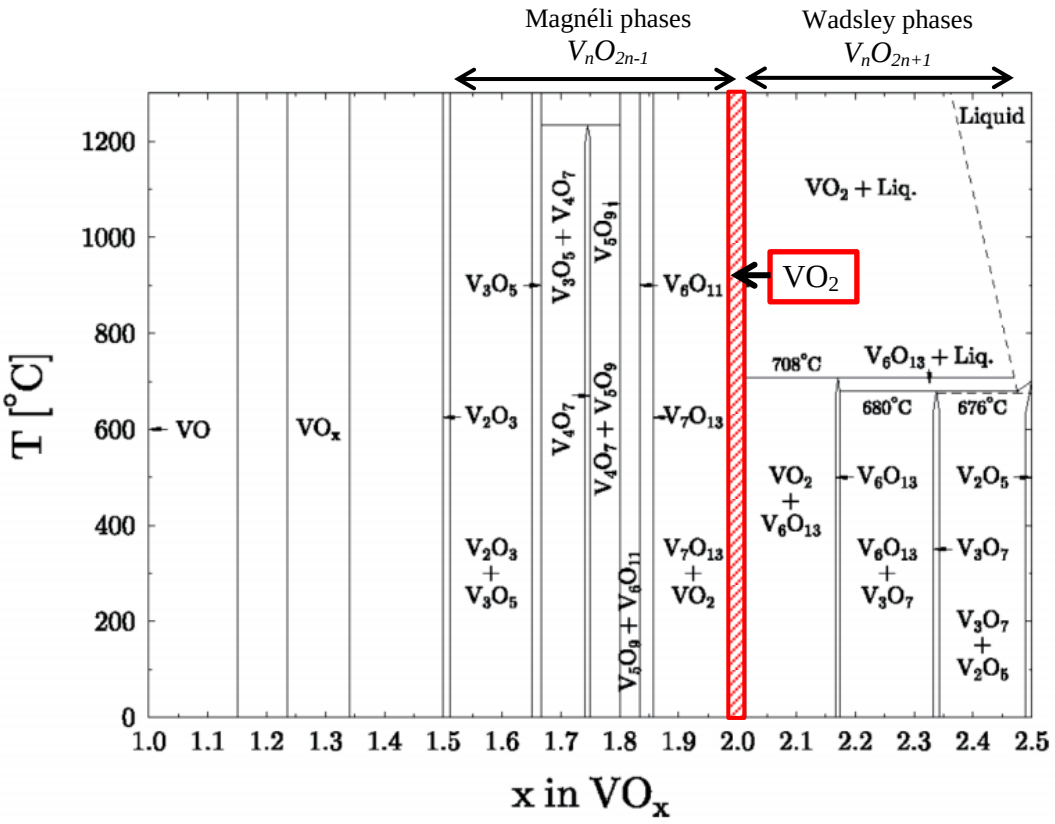

Figure 2.1: Vanadium–oxygen phase diagram showing VOx in the range 1 ≤ x ≤ 2.5, variation from Katzke et al. [3].

As shown in figure 2.1, vanadium oxides have a degree of oxidation from +II (phase VO for x < 1,15) to +V (phase V_2O_5 for x > 2.5). Vanadium pentoxide (V_2O_5) is the most chemically stable phase and presents a first order transition when the temperature surpasses 276ºC. First order transitions are characterised by a change of phase when the material surpasses a critical temperature value (T_c). In addition to vanadium pentoxide, vanadium dioxide (VO_2) and vanadium sesquioxide (V_2O_3), there are nearly twenty other stable oxide phases. These have no interesting phase transitions compared to VO_2 their phase diagrams are similar to those of VO_2 and V_2O_3 (Figure 2.2), creating a special difficulty in growing thin films of VO_2. [4, 5]. Given the amount of intermediate compounds, producing films of a concrete oxygen composition has to be done with rigorous control to avoid polyphased films [6].

These other phases can be put in two groups. In one hand, the first group follows the following stoichiometric formula: V_nO_{2n+1} and exists between V_2O_5 and VO_2. The phases comprised in it are called Wadsley phases. On the other hand, the second group follows the formula: V_nO_{2n-1}, exists between VO_2 and V_2O_3 and the phases in it are called Magnéli phases [5] (Figure 2.3). All of these

phases (except one), both in the first and in the second group, exhibit a change from a metallic to a semiconductor behaviour.

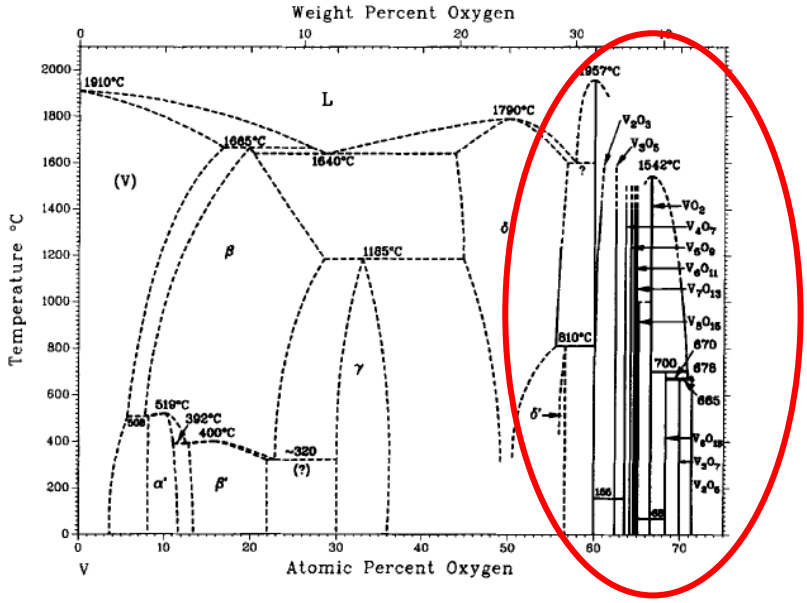

Figure 2.2: Vanadium-oxides phase diagram [7].

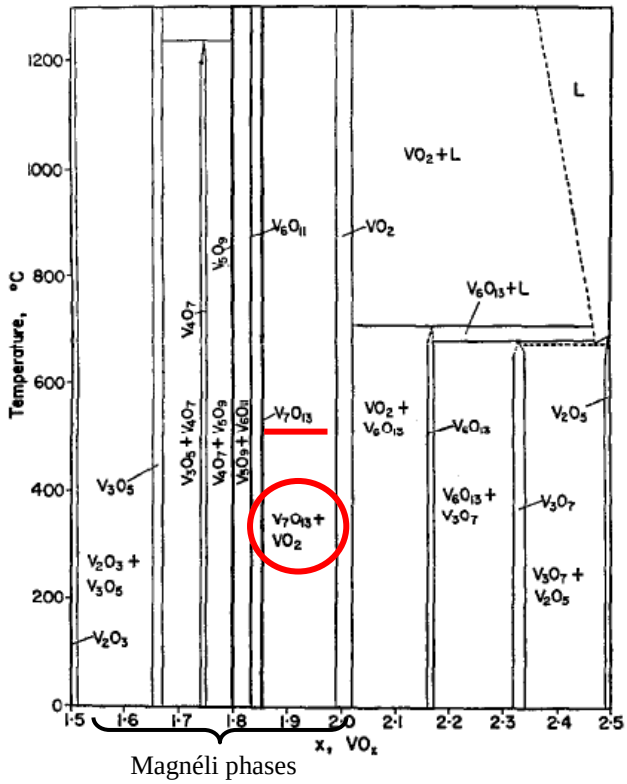

Figure 2.3: Phase diagram [8] combined with KACHI and ROY'S data [9] and the present work.

2.1.1 Magnéli phases

The Magnéli phases, of generic formula M_nO_{2n-1} (with M being: V, Ti…), have been largely studied to understand the first order phase transitions of the type metallic/semiconductor (MIT: Metal to Insulator Transition) [10]. The vanadium Magnéli phases V_nO_{2n-1} are defined by U. Schwingenschlögl and V. Eyert [5] with the following formula:

$$V_nO_{2n-1} = V_2O_3 + (n-2)VO_2, \text{ with } 3 \leq n \leq 9$$

Their MIT transition temperatures T_c are detailed in table 2.1.

Table 2.1: Magnéli phases and their correspondent phase transition temperatures.

Vanadium Magnéli phase	T_c
V_3O_5	-156
V_4O_7	-23
V_5O_9	-138
V_6O_{11}	-103
V_7O_{13}	No MIT
V_8O_{15}	-203
V_9O_{17}	-198

All of these transitions are reversible, changing from semi-conductors at low temperature to metallic at high temperature, accompanied by a change in the crystalline nano-structure. These phases experience, thus, a change in their magnetic [11], mechanical, optical and electrical properties with temperature. V_7O_{13} is the only vanadium oxide which is always metallic [5, 12], although its magnetic properties do change with the transition.

The different properties of Magnéli's phases have been studied and used in fields like tribology for applications as lubricants at high temperature, protecting the coatings from corrosion and limiting their friction [13].

2.1.2 Wadsley phases

Vanadium oxides of chemical composition V_nO_{2n+1} are comprised in between VO_2 and V_2O_5. Nowadays, only V_6O_{13}, V_4O_9 and V_3O_7 have been synthesised in the form of powder or crystals. Most of these phases, as the Magnéli ones, have a semi-conductor/metal transition and their properties change with it.

2.2 Vanadium dioxide (VO_2)

Vanadium dioxide is of particular interest since F.J. Morin discovered its reversible phase transition near room temperature in 1959 [14] and is also attractive for its optical commutation in the infrared interval. The challenge relies in obtaining the exact compound, due to the need of a rigorous control of the oxygen content (VO_x with $1{,}98 < x < 2{,}03$), as can be observed in figure 2.3.

2.2.1 Important nano-structures

VO_2 can crystallize in different stable phases: VO_2(M1) for monoclinic one, VO_2(M2) for the base centred monoclinic phase and metastable VO_2(T) for the triclinic phase, in function of the method of growth and the experimental parameters. The high temperature phase VO_2(R) and low temperature phase (M1) are described below. The VO_2(M2) phase is not described because it can only be achieved enhancing doping, which is not studied in this work.

a) The high temperature phase VO_2 (R)

At a temperature higher than T_c, VO_2 is characterised by its rutile quadratic phase nano-structure, noted VO_2 (R) and represented in Figure 2.4. Its mesh parameters are [15]:

$$a_R = b_R = 0{,}45546 \text{ nm}$$

$$c_R = 0{,}28528 \text{ nm}$$

In this nano-structure, the vanadium atoms of valence +IV are surrounded by six oxygen atoms of valence –II, creating a VO_6 octahedron. It should be noted that in this high temperature nano-structure there is no metallic vanadium-vanadium bonding and there is only one interatomic distance

from the central vanadium atom to the mesh and the six oxygen atoms. In this phase, VO_2 (R) dioxide of vanadium presents a metallic behaviour and rests opaque to infrared rays.

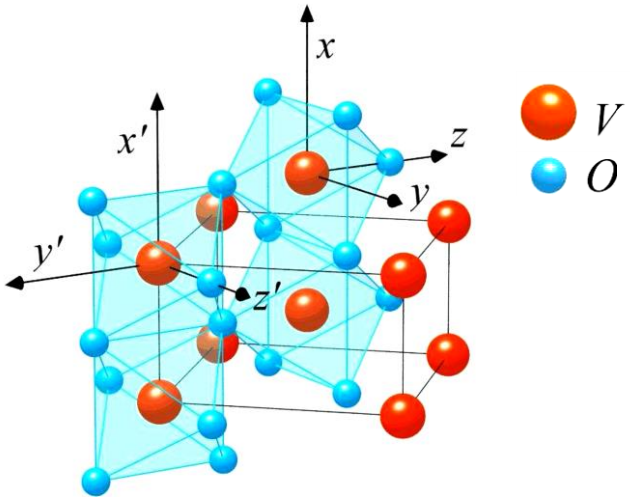

Figure 2.4: Crystalline quadratic rutile nano-structure of VO_2 at high temperature, noted VO_2(R)[16].

b) The low temperature phase VO_2 (M1)

At a lower temperature than 68ºC, vanadium dioxide experiences a sudden structural transition and changes from its rutile quadratic phase to its monoclinic low temperature nano-structure, noted VO_2 (M1) and represented in Figure 2.5. This phase can be seen as a lengthening in the c_R axis of two superposed meshes of the quadratic rutile nano-structure, followed by torsion. The vanadium atoms shift slightly in relation to their original positions and are no longer aligned with each other along the c_R axis (Figure 2.5).

Metallic V-V bonds 0, 2619 nm long are formed in zig-zag, by pairs, modifying the mesh parameters from the original rutile nano-structure, according to J. M. Longo and P. Kierkegaard [17], with the following values:

$$a_{M1} = 2c_R = 0{,}57517 \text{ nm}$$

$$b_{M1} = 0{,}45378 \text{ nm}$$

$$c_{M1} = a_R - c_R = 0{,}53825 \text{ nm}$$

$$\beta_{M1} = 122{,}646°$$

Also, in this phase it is important to note that there are two different vanadium-oxygen interatomic distances: V-O_1 and V-O_2, of corresponding lengths 0,177 nm and 0,201 nm.

Monoclinic VO_2 presents semiconductor behaviour and rests transparent to infrared rays.

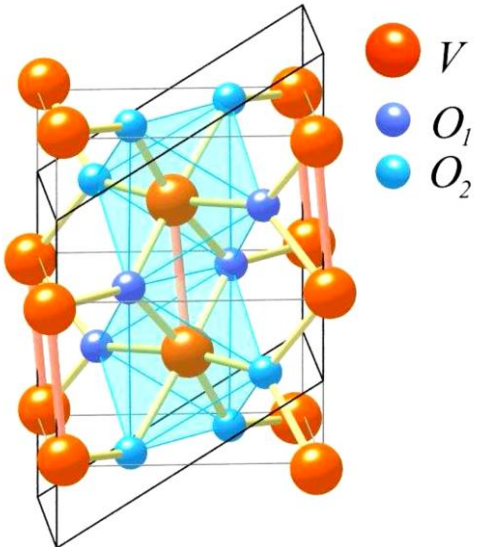

Figure 2.5: Monoclinic nano-structure of VO_2 at low temperature, noted VO_2 (M1) [16].

2.2.2 Physical properties

The phase transition in VO_2 carries with it a change of the resistivity of the material [18, 19]. In the low temperature interval, the monoclinic VO_2 (M1) phase has a bandgap of 0.6 eV at 25 °C and converts into metallic rutile in the high temperature phase VO_2 (R) at 68 °C, resulting in a brusque change of the bulk electrical resistivity, from two to six orders of magnitude. The VO_2 MIT is revealed in an abrupt interfacial transition of current across a VO_2 barrier interface forming a tunnel junction. In a first tunnel junction form, a two orders of magnitude rough change in contact resistivity induced by the bulk MIT is shown in VO_2-metal contact nano-structures [14, 20]. The working zone of VO_2 is 5.2eV (25 °C) −5.3eV (90 °C). The brusque change in current across the VO_2 interface is due to the change in free carriers in bulk VO_2 across the MIT [21].

The optical properties of VO_2, such as reflectance [22], emission [23] or transmittance [24], are also modified with the phase transition. Being this transition reversible and of first order, there is a mixture of oxide phases that present a hysteresis loop. When VO_2 is heated, the material goes from its metallic phase VO_2(R) to its semi-conductor phase VO_2 (M1). When cooling, the semiconductor phase

will germinate into the metallic phase but at a different temperature [25]. The change in the optical properties also brings a change in the optical index *n* (refraction index) and *k* (extinction index), mostly in the infrared domain, as shown in the work of F. Guinneton [25]. S. Mukherjee and A.K. Pal recently studied the magnetic properties of VO_2 nano-crystals in a silicon matrix, demonstrating a magnetic transition, of the type superparamagnetic-ferromagnetic, at the temperature of -263 ºC.

In this work we will focus on the change of resistivity in VO_2 as our main interesting property. To understand why there is a change in all these properties, it is necessary to comprehend the electronic bands nano-structure of VO_2 in function of temperature.

2.2.3 Semiconductor-to-metal transition (MIT)

Most of the metal oxides near to vanadium crystallise into a rutile nano-structure. However, in function of their electronic configuration, their phase transition occurs differently. Vanadium is situated in between titanium (Ti) and chromium (Cr) in the periodic table. Titanium oxide TiO_2 ($3d^0$) crystalizes into a rutile nano-structure with a big band gap of energy, becoming an insulator. Chrome oxide CrO_2 ($3d^2$) always stays metallic, although it has a paramagnetic-ferromagnetic transition when crystalizing into the rutile phase. As vanadium dioxide ($3d^1$) is situated in between them both, it presents an intermediate behaviour in its semiconductor-metal transition [26].

As it has been said, the bands nano-structure of VO_2 change in function of temperature [27]. In one hand, at low temperature the compound is in a semi-conductor state, so there is a gap in between the valence band (which is full of electrons) and the conduction band (empty of electrons). This gap is the consequence of the strong V-V metallic bond at low temperature, which does not permit the fulfilment of the band. On the other hand, at high temperature the formation of a rutile nano-structure erases the metallic bonds, making the energy gap disappear. The material then becomes metallic and the electrons in the valence band can easily move to the conduction band and form electron-hole pairs in both bands. The appearance of these pairs of charges explains the decrease of transmittance and the rise of reflectivity, given the compound is in its metallic state.

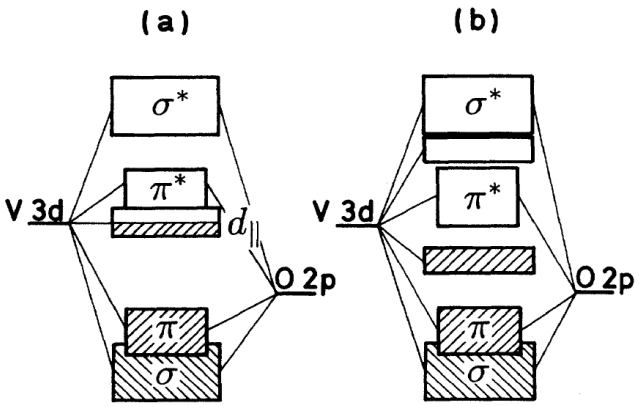

Figure 2.6: Scheme of the bands nano-structures of VO_2, at high temperature rutile nano-structure (a) and at low temperature when distorting rutile to monoclinic nano-structure (b) [28].

After the description of the bands nano-structures, the different ways to synthesis VO_2 thin films are detailed in the following part of this chapter.

2.3 Vanadium dioxide thin films synthesis methods

Many methods can be used to elaborate VO_2 thin films. All of them have three principle steps in the formation of any deposit:

1. Synthesis of the material to be deposited:
   a) Transition from a condensed phase (solid or liquid) to the vapour phase
   b) For deposition of compounds, a reaction between the components of the compound, some of which may be introduced into the chamber as a gas or vapour.
2. Transport of the vapours between the source and substrate.
3. Condensation of vapours and gases followed by film nucleation and growth.

In this section, a brief review of all the methods used to synthesise thin films of VO_2 till the present is given. In the end, the method chosen for this work is presented, along with the reasons why. Figure 2.7 shows a summary of all the soon to be described methods.

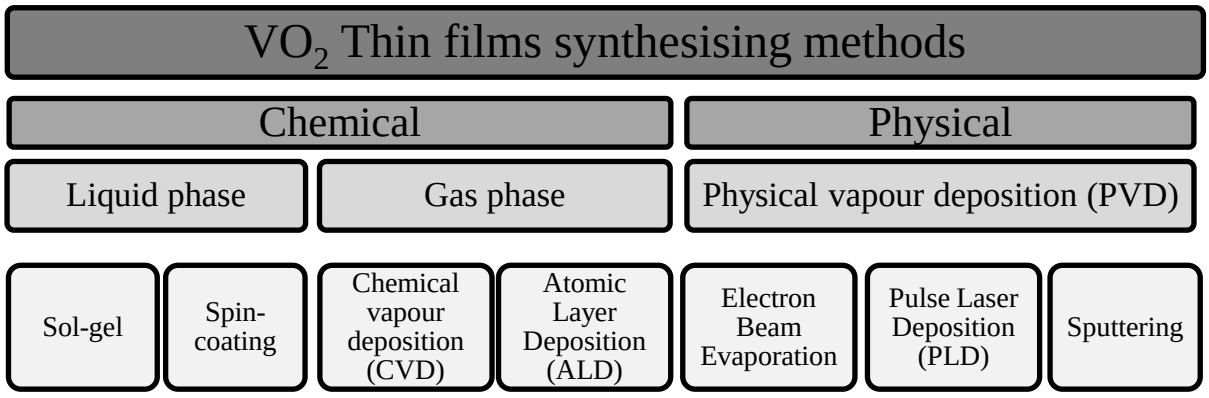

Figure 2.7: Scheme of VO_2 thin films synthesising methods.

2.3.1 Sol-gel

This chemical synthesising method [29] uses metallic vanadium powder and oxygenated water as precursor. The solution is heated up to 50 ºC to obtain gel at room temperature. Finally, the gel is heated up to 750 ºC for 2 hours inside a vacuum oven. VO_2 thin films with a 200 nm thickness and grains sizes in between 100 nm and 500 nm are created. The surface morphology shows a powdery look, as can be observed in N. Wang's work [30].

2.3.2 Spin-coating

When mixing V_2O_5 powder with an organic solution, a gel is obtained. This gel is then rotated and annealed on a mica substrate, inside a tubular oven between 440-540ºC for 30 minutes and in a nitrogen atmosphere. The resulting surface and grains' size of the VO_2 films depend mainly on the annealing temperature [31]. The phase transition temperature *Tc* increases to 75ºC, being higher than the one usually obtained with other methods (68ºC).

2.3.3 Chemical vapour deposition (CVD)

B. W. Mwakikunga's article presented the synthesis of VO_2 by ultrasonic spray pyrolysis for the first time [32]. A precursor solution of ammonium meta-vanadate, enriched with vanadium tri-chloride, was found to be one of the most suitable starting solutions from which droplets were

generated by an ultra-sonicator operated at 1.7 MHz. A powdery surface and a wide range of grains sizes can be observed in his work.

2.3.4 Atomic layer deposition (ALD)

ALD is a chemical gas phase thin film deposition method based on sequential, self-saturating surface reactions. The ALD method was developed for commercial use in Finland in the mid-1970s by Dr Tuomo Suntola and co-workers. [33-37]. Two or more precursor chemicals, each containing different elements of the materials being deposited, are introduced to the surface separately, one at a time. Each precursor saturates the surface forming a monolayer of material [38A].

Initially developed to produce thin film electroluminescent (TFEL) flat panel displays, it is now used for multiple other industrial applications such as semi-conductor devices manufacturing, due to its high control in surface precision and the ability of creating ultra-thin films. This technique has also been used to study VO_2 thin films [39]. However, ALD processes with vanadium oxides mostly result in the growth of V_2O_5 [40].

2.3.5 Physical vapour deposition (PVD)

Physical vapour deposition (PVD) gathers a variety of vacuum deposition methods which are based in the condensation of a vaporized form to deposit thin films of a desired material onto various substrate surfaces.

a) Electron Beam Evaporation (EBPVD)

A target anode is bombarded with an electron beam given off by a charged tungsten filament under high vacuum. The electron beam causes atoms from the target to transform into the gaseous phase. These atoms then precipitate into solid form, coating everything within line of sight in the vacuum chamber with a thin layer of the anode material.

Recent studies have found Electron Beam Evaporation to be a highly suitable method to create VO_2 thin films [41, 42]. Active photonic devices incorporating VO_2 deposited by this technique perform at least as well, if not better, than those produced by pulsed laser deposition [43]. In addition, the near-perfect stoichiometry of the deposited films as a result of the powder precursor

requires short annealing times and produces films with a smooth morphology. Converting these films to high-quality VO_2 requires only a short time under the conditions at which VO_2 is the preferred oxide [44].

In spite of the attractive laser evaporation approaches, for VO_2 it suffers from the following limitations [38B]:

- Complex transmitting and focusing systems need to be employed to direct the beam from the laser, located outside the vacuum system, onto the evaporator, placed inside the system. This involves special optical path designs and increases the cost of the set-up. Also, a window material which efficiently transmits the wave-length band of the laser must be found and mounted in such a way that it is not rapidly covered up by the evaporated material.
- Energy conversion efficiency is very low, around 1-2%.
- The size of the deposited film is small (10-20mm or 0.4-0.8 inches in diameter), due to the small size of the laser impact spot.
- The 'splashing effect' [45], which involves the production of micro-particles between 0,1 and 10μm in size, diminishes the quality of the films.

b) Pulsed laser deposition (PLD)

There are many studies using PLD to create VO_2 thin films [46, 47 and 48]. This PVD technique uses a high-power pulsed laser beam focused inside a vacuum chamber to hit the target of the material being deposited. This material is then vaporized in a plasma environment which deposits it as a thin film on the substrate. This process needs of ultra-high vacuum or the presence of a reactive gas, such as oxygen, commonly used when depositing oxides to fully oxygenate the deposited films.

c) Sputtering methods

Sputtering was first discussed in the literature by W.R. Grove, in 1854 [49], and is now widely used to deposit thin films on substrates [50, 51]. Sputtering describes the ejection of atoms by the bombardment of a target with energetic particles such as ions. The ejected atoms result in a vapour due to a purely physical process and impact on the substrate or vacuum chamber. The method and precise

details on the process parameters are described in Peter M. Martin's *Handbook of Deposition Technologies for Films and Coatings* [38C], also, the interactions between the ions and the target are largely studied in many review articles.

Two approaches can be followed to produce ions and sputter the target materials. Ion guns are more often used in surface analytical techniques, such as secondary ion mass spectrometry (SIMS), or to bombard the substrate during thin films deposition [52]. Another source of ions is plasma. By applying a high negative voltage to the cathode, i.e. the target, positively charged ions are attracted from the plasma towards the target. The ions gain energy in the electric field and bombard the target with sufficient energy to initiate sputtering. For efficient momentum transfer, the atomic weight of the sputtering gas should be close to the atomic weight of the target. Therefore, neon is preferable for sputtering light elements, whilst krypton or xenon are used for heavy elements. Argon is very often used too.

The advantages of sputter deposition are the low substrate temperature used and that even materials with very high melting point are easily sputtered. Also, the film and the target have a similar composition. Sputtered films tend to have a better adhesion on the substrate than evaporated films. In addition, the target contains a significant amount of material, reducing the maintenance and making this method suitable for ultra-high vacuum applications. The target is typically water cooled to avoid over-heating and the sputter is compatible with reactive gases such as oxygen or nitrogen. Sputtering can be performed top-down, while evaporation must be performed bottom-up. Moreover, complex processes like epitaxial growth are possible.

Some disadvantages of sputtering are that the process is more difficult to combine with a lift-off for structuring the film. This is because the diffuse transport, characteristic of sputtering, makes a full shadow impossible. Thus, one cannot fully restrict where the atoms go, which can lead to contamination problems. Also, active control for layer-by-layer growth is difficult compared to pulsed laser deposition. Finally, inert sputtering gases can be trapped in the film as impurities.

The most common approach for growing thin films by sputter deposition is the use of a magnetron source. Enhancing a discharge, plasma is created and the positive ions in it bombard the

target. Magnetrons can be powered in several ways. Direct current (DC), pulsed DC and high-power impulse magnetron sputtering (HIPIMS) can be used for conductive targets. Otherwise, radio frequency (RF) can be used for non-conductive ones. Since sputtering is a purely physical process, to have chemical reactions a reactive gas is needed with the plasma. This method is then called reactive sputtering (RRSP) [38D].

In this work, DC Magnetron sputtering is used to deposit thin films of VO_2 because of its film homogeneity, expandability to larger substrate sizes and efficiency of deposition when compared to the other methods [53]. It is also the simplest and least expensive way to operate the magnetron. Plasma will be ignited with argon gas and an external DC generator. Glass and silicon will be the materials used as substrates to allow the study of different properties of the films obtained. At the same time, the GLAD (GLancing Angle Deposition) technique will be used during the sputtering, allowing the growth of a large variety of morphologies. Finally, also reactive sputtering with oxygen will be carried out to study more porous vanadium oxides nano-structures. The nano-structure of magnetron sputter-deposited films is defined by the identity of the particles arriving at the substrate, their fluxes and the energy per particle [38D].

In the following section 2.4, the GLAD technique is fully described.

2.4 The GLAD technique

In 1997, Robbie and Brett [54] introduced for the first time the term GLAD (GLancing Angle Deposition). From then onwards, films made under inclined incidence and with either fixed or mobile substrate started to be widely studied. Firstly, the general principle of this technique is explained, along with some experimental schemes. After, the possible nano-structures to be achieved by GLAD are described.

2.4.1 Principle

The GLAD technique relies in the ability of changing the position of the substrate in relation to the vapour source. When the atoms impact on the substrate, they gather to form growth germs. At

the same time, as the germs increase their size, the shadowing effect makes its appearance. In figure 2.8 this effect is schemed in a simple way.

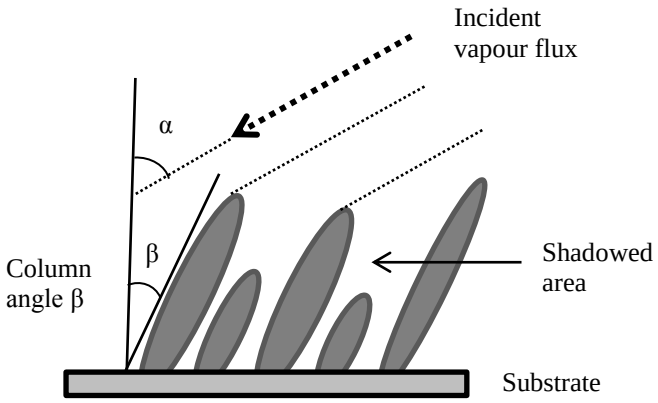

Figure 2.8: Growth of inclined columns under the Shadowing effect.

Due to the shadowing effect, there is a decrease in the density of the films. Conventionally, the angles are measured with reference to the substrates normal. The target (vapour source) stays fix, whilst the substrate can be orientated in the space. The centre of the source is usually aligned with the substrate's centre, allowing orientating the latter easily. This way, there are two possible rotations (Figure 2.9).

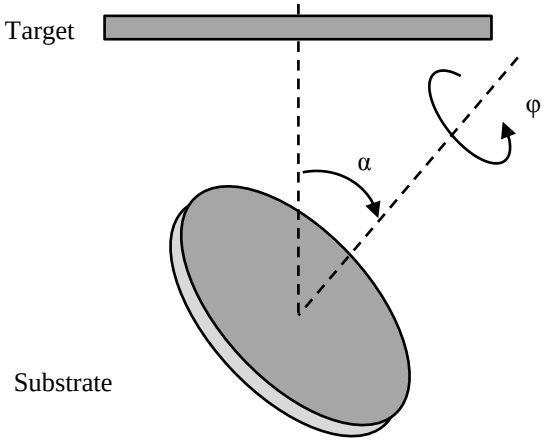

Figure 2.9: Possible substrate rotations in a GLAD deposition.

The α rotation can oscillate between -90º and 90º, corresponding to the atoms' incidence angle (approximately). On the other hand, the rotation φ can vary 360º in both senses (clockwise or

anticlockwise). Φ corresponds to the azimuthal angle, which, allows controlling the nano-films' nano-architecture without modifying the substrate's position towards the source.

The shadowing effect, surface diffusion and atom's angular distribution in the flux contribute to the growth of the columns with an angle β different to α. It is known that there is a fixed relationship between these two angles for a given set of deposition conditions. This relationship is complex and poorly understood, but there have been some attempts at understanding and quantifying it [55]. The empirical tangent rule [56] (1) is a simple relationship based on aproximately normal deposition and gives very poor results for α greater than about 50°. On the contrary, the relationship based on geometrical analysis proposed by Tait *et al*.[57] (2) gives much better results for highly oblique angles.

$$\mathrm{Tan}(\beta) = \frac{1}{2}\tan(\alpha) \qquad \textbf{(1)}\ \text{Tangent rule}$$

$$\beta = \alpha - \sin^{-1}\left[1 - \frac{\cos\alpha}{2}\right] \qquad \textbf{(2)}\ \text{Tait's rule}$$

However, there are many other experimental parameters a part from the incidence angle that influence β and therefore disagree with the formulae: Work pressure, surface pollution, atom diffusion, deposition speed, temperature, nature of materials used and even the polarisation of the substrate during the deposition.

This shows the complexity in determining the angle β of the columns in advance. In this work, this angle will be determined experimentally with measuring it after the depositions.

2.4.2 Nano-architectures produced with GLAD

The substrate's orientation in front of the target, as well as the procedures available within GLAD, allow the manufacture of a large number of nano-architectures. In this work we will work with the following three: Inclined columns, zig-zags and spirals.

1) Inclined columns

When the substrate is inclined so that the incident angle α is different than zero and stays in the said position during all the deposition, the nano-structure of the film is of inclined columns (Figure 2.10 a)). These columns will grow with an angle β, which depends on several factors, already

described in section 2.4.1. The shadowing effect takes place in one unique direction. However, in the early first stages, it has been proven [58, 59 and 55] that the growth is perpendicular to the substrate's surface. This type of nano-structure has been applied to many materials before:

-Pure elements such as: Iron [60, 61], germanium [62], chrome [39], silicium [63], nickel [64] and vanadium.

-Oxides such as: WO_3 [65], TiO_2 [66] and ZrO_2 [67].

2) Zig-zags

To achieve zig-zag nano-structures (Figure 2.10 b)), there has to be a variation in the incidence angle α during the deposition. To obtain symmetrical zig-zags [68] there has to be a periodical variation of 180º (from +α to –α), depending on the number of zig-zags desired. The azimuthal angle φ relies constant.

3) Spirals

To obtain 3D nano-structures such as spirals, both the incidence angle α and the azimuthal angle φ have to vary (Figure 2.10 c)). These nano-structures can be done in plenty of different ways, but to create continuous spirals the angle variation has to be constant, as observed in K. Robbie's MgF_2 films [55].

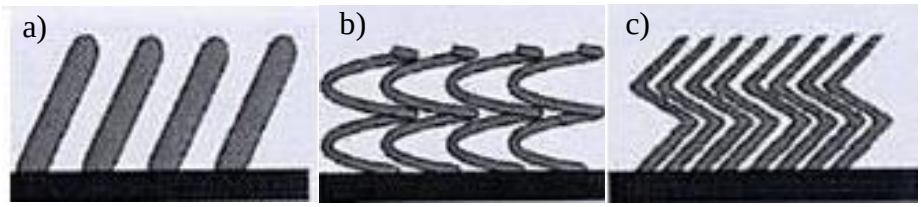

Figure 2.10: Scheme of the three nano-architectures described: a) Inclined columns b) Zig-zags and c) Spirals

2.4.3 Properties of the films

Films prepared with GLAD have particular structural, mechanical, optical and conductivity properties.

a) Structural properties

i. Density

Films prepared by PVD processes tend to have very high density, approximately 80 to 95% of the bulk. GLAD allows diminishing this density and, therefore, increase the porosity of the film. Furthermore, with incidence angles higher than 70º, the density decreases strongly. Robbie *et al*. [69] achieved density values of a 10% of the bulk in CaF_2 films.

A high rate of porosity is interesting because it increases the material's contact surface with the atmosphere, allowing the film's application in gas and humidity captors [70] and in photovoltaic solar cells [71, 72].

ii. Surface appearance

Modifying the nano-architecture of the film, it is possible to control the morphology of the surface [73]. This way, we can change the roughness of the film in function of the incidence angle, control anisotropic roughness and create a periodic morphology.

iii. Crystallography

When we vary the angle of incidence, the mobility of the atoms on the substrate is highly affected. For incidence angles higher than 40º, Allouach *et al.* observed a variation of the crystalline nano-structure for epitaxial copper films [74]. Karabacak *et al.* even arrived to choose the growth orientation of tungsten phases α and β in function of the incidence angle [75].

b) Mechanical Properties

Zig-zag and spiral nano-structures have great resemblances with springs and column nano-architectures increase the elasticity in comparison to classical films [76]. Also, it is possible to change the Young modulus and hardness of zig-zag films by varying the number of periods or length of the segments [77]. However, this work will not focus on the mechanical properties of the films created.

c) Optical properties

Due to the anisotropy presented in GLAD films, these have been very interesting to the optical sector [78]. Filtering the light in reflexion and birefringence of inclined columns and zig-zag nano-structures are the most important optical properties used, although these are not studied in this work.

d) Conductivity

Apart from photo-catalytic and photonic conductivity, the most interesting property of vanadium dioxide films is their electric conductivity, which will be intensely studied in this work. This conductivity depends of the film's nano-structure, its porosity, anisotropy and temperature [79, 80 and 81].

Bibliography of chapter 2

[1] Dongyang Chen, Michael A Hickner, Ertan Agar and Caglan Kumbur E 2013 Optimized Anion Exchange Membranes for Vanadium Redox Flow Batteries *ACS Applied Materials & Interfaces* **5(15)** 7559-7566.

[2] Niesert A, Hanrath M, Siggle A, Jansen M and Langer K 2002 Theoretical study of the polarized electronic absorption spectra of vanadium-doped zircon *Journal of Solid State Chemistry* **169** 6-12.

[3] Katzke H, Tolédano P and Depmeier W 2003 *Phys. Rev. B* **68(2)** 024109.

[4] Griffith Ch and Eastwood H K 1974 Influence of Stoichiometry on Metal-Semiconductor Transition in Vanadium Dioxide *Journal of Applied Physics* **45(5)** 2201-2206.

[5] Schwingenschlogl U and Eyert V 2004 The vanadium Magneli phasesV_nO_{2n-1} *Annalen Der Physik* **13(9)** 475-510.

[6] Dillon R O, Le K and Ianno N 2001 Thermochromic VO_2 sputtered by control of a vanadium-oxygen emission ratio *Thin Solid Films* **398-399** 10-16.

[7] Wriedt H A 1989 The O-V (Oxygen-Vanadium) System *Bulletin of Alloy Phase Diagrams* **10(3)** 271-277.

[8] Kosuge K 1967 The phase diagram and phase transition of the V_2O_3-V_2O_5 system *J. Phys. Chem. Solids* **28** 1613-1621.

[9] Kachi S and Roy R 1965 Second Quarterly Report on Crystal Chemistry Studies *Pennsylvania State University* **4.**

[10] Marwitz C, Stegemann B, Breitkitz M, Spaltmann D, Kloss H, Woydt M and Sturm H 2011 Correlations of adhesion force and electrical conductivity in Magnéli-type vanadium oxydes and highly oriented pyrolytic graphite *Surface Science* **605** 1271-1274.

[11] Marezio M, Gauzzi A, Licci F and Gilioli E 2000 Can the nano-structure of the Ti and V Magnéli binary oxides host superconductivity? *Physica C: Superconductivity* **338** 1-8.

[12] Pergament A, Stefanovich G and Andreeev V 2013 Comment on "Metal-insulator transition without structural phase transition in V_2O_5 film" [Appl. Phys. Lett. 98, 131907 (2011)] *Applied Physics Letters* **102(17)** 176101.

[13] Fateh N, Fontalvo G A, Gassner G and Mitterer C 2007 Influence of high-temperature oxide formation on the tribological behaviour of TiN and VN coatings *WEAR* **262** 1152-1158.

[14] Morin F 1959 Oxides Which Show a Metal-to-Insulator Transition at the Neel Temperature *Phys.Rev.Lett.* **3** 34.

[15] Zhen-Fei L, Zhi-Ming W, Xiang-Dong X, Tao W and Ya-Dong J 2010 Study of nanocrystalline VO_2 thin films prepared by magnetron sputtering and post-oxidation *Chinese physics B* **19(10)** 106103.

[16] Eyert V 2002 The metal-insulator transitions of VO_2: a band theoretical approach *Ann. Phys. (Leibniz)* **11(9)** 650-702.

[17] Longo J M and Kierkegaard P 1970 Thermodynamics of strained vanadium dioxide single crystal *Acta chimica Scandinavica* **24** 420-426.

[18] Lappalainen J, Heinilehto S, Saukko S, Lantto V and Jantunen H 2008 Micronano-structure dependent switching properties of VO_2 thin films *Sensors and actuators A* **142** 250-255.

[19] Park K M, Yi S, Moon S and Im S 2001 Optimum oxygen concentration for the optoelectronic properties of IR sensitive VO_x thin films *Optical Materials* **17** 311-314.

[20] Rosevear W H and Paul W 1973 Hall effect in VO_2 near the semiconductor-to-Metal Transition *Phys. Rev. B* **7** 2109.

[21] Martens K *et al.* 2012 The VO_2 interface, the metal-insulator transition tunnel junction, and the metal-insulator transition switch On-Off resistance *Journal of Applied Physics* **112(12)** 124501.

[22] Golan G, Axelevitch A, Sigalov B and Gorenstein B 2003 Metal-insulator phase transition in vanadium oxide films *Microelectronics Journal* **34** 255-258.

[23] Guinnetton F, Sauques L S, Valmalette J C, Cros F and Gavarri J R 2001 Comparative study between nanocrystalline powder and thin film of vanadium dioxide VO_2: electrical and infrared properties *Journal of Physics and Chemistry of Solids* **62** 1229-1238.

[24] Hua-Kuo C, Hsin-Chin H, Thomas C-K Y and Sea-Fue W 2004 The preparation and characterization of transport nano-sized thermochromic VO_2-SiO_2 films from the sol-gel process *Journal of Non-Crystalline Solids* **347** 138-143.

[25] Guinneton F, Sauques L, Valmalette J C, Cros F and Gavarri J R 2004 Optimized infrared switching properties in thermochromic vanadium dioxide thin films: role of deposition process and micronano-structure *Thin Solid Films* **446** 287-295.

[26] Corvisier A 2014 *Élaboration par pulverisation magnetron reactive d'une couche thermochrome à base de dioxide de vanadium. Application à la regulation passive de la temperature de panneaux solaires* (Doctoral Dissertation) Université de Lorraine, Nancy 32.

[27] Caruther E and Kleinman L 1973 Energy Bands of Semiconducting VO_2 *Physical Review B* **7(8)** 3753-3760.

[28] Abbate M, Groot F M F, Fuggle J C, Ma Y J, Chen C T, Sette F, Fujimori A, Ueda Y and Kosuge K 1991 Soft-x-ray-absorption studies of the electronic-nano-structure changes through the VO_2 phase transition *Physical Review B* **43(9)** 7263-7266.

[29] Nag J and Haglund Jr. R F 2008 Synthesis of vanadium dioxide thin films and nanoparticles *Journal of Physics: Condensed Matter* **20** 264016-264030.

[30] Wang N, Magdassi S, Mandler D and Long Y 2013 Simple sol-gel process and one-step annealing of vanadium dioxide thin films: Synthesis and thermochromic properties *Thin Solid Films* **534** 594-598.

[31] Wu J, Huang W, Shi Q, Cai J, Zhao D, Zang Y and Yan J 2013 Effect of annealing temperature on thermochromic properties of vanadium dioxide thin films deposited by organic sol-gel method *Applied Surface Science* **268** 556-560.

[32] Wakufuwa Mwakikunga B, Sideras-Haddad E and Maaza M 2007 First synthesis of vanadium dioxide by ultrasonic nebula-spray pyrolysis *Optical Materials* **29** 481-487.

[33] Suntola T and Antson J 1977 US Patent No. 4,058,430.

[34] Suntola T, Pakkala A P and Lindfors S G 1980 SID 80 Digest **11** 108.

[35] Suntola T, Pakkala A P and Lindfors S G 1983 US Patent No. 4,389,973.

[36] Suntola T, Pakkala A P and Lindfors S G 1983 US Patent No. 4,413,022.

[37] Ritala M and Leskelä M 2002 *Handbook of Thin Film Materials* **1** Ed. Nalwa H S, Academic Press San Diego 103-159.

[38] **[38A]** Martin P M 2010 *Handbook of Deposition Technologies for Films and Coatings* Ed. Ron Bunshaw (Third Edition), UK: Elsevier Inc. 364-388.

[38B] Martin P M 2010 *Handbook of Deposition Technologies for Films and Coatings* Ed. Ron Bunshaw (Third Edition), UK: Elsevier Inc. 147.

[38C] Martin P M 2010 *Handbook of Deposition Technologies for Films and Coatings* Ed. Ron Bunshaw (Third Edition), UK: Elsevier Inc. 253-294.

[38D] Martin P M 2010 *Handbook of Deposition Technologies for Films and Coatings* Ed. Ron Bunshaw (Third Edition), UK: Elsevier Inc. 253-254.

[39] Rampelberg G, Schaekers M, Martens K, Xie Q, Deduytsche D, De Schutter B, Blasco N, Kittl J and Detavernier C 2011 Metal transition in thin VO_2 films grown by ozone based atomic layer deposition *Applied Physics Letters* **98** 162902.

[40] Musschoot J, Deduytsche D, Poelman H, Haemers J, R. Vanmeirhaeghe R L, Van den Berghe S, and Detavernier C and Electrochem J 2009 *Soc.* **156** 122.

[41] Marvel R E, Appavoo K, Choi B K, Nag J and Haglund Jr. R F 2013 Electron-beam deposition of vanadium dioxide thin films *Appl. Phys. A* **111** 975-981.

[42] Leroy J, Bessaudou A, Cosset F and Crunteanu A 2012 Structural, electrical and optical properties of thermochromic VO_2 thin films obtained by reactive electron beam evaporation *Thin Solid Films* **520** 4823-4825.

[43] Ryckman J D, Diez-Blanco V, Nag J, Marvel R E, Choi B K Haglund Jr. R F and Weiss S M 2012 *Opt. Express* **20**(12) 13215.

[44] Suh J Y, Lopez R, Feldman L C, Haglund Jr. R F 2004 *J Appl. Phys.* **96** 1209–1213.

[45] Wu X D, Dijkkamp D, Olgale S B Ina, A, Chase E W, Miceli P F *et al.* 1987 *Appl. Phys. Lett.* **51** 861.

[46] Sakai J, Zaghrioui M, Phuoc V T, Roger S, Autret-Lambert C and Okimura K 2013 Pulsed laser-deposited VO_2 thin films on Pt layers *Journal of Applied Physics* **113** 123503.

[47] Rúa A, Cabrera R, Coy H, Merced E, Sepúlveda N and Fernández F E 2012 Phase transition behavior in microcantilevers coated with M1-phase VO_2 and M2-phase VO_2:Cr thin films *Journal of Applied Physics* **111** 104502.

[48] Okimura K, Sakai J and Ramanathan S 2010 In situ x-ray diffraction studies on epitaxial VO_2 films grown on c-Al_2O_3 during thermally induced insulator-metal transition *Journal of Applied Physics* **107** 063503.

[49] Grove W R and Phil Trans R 1852 *Soc. Lond.* **142** 87-101.

[50] Okimura K, Watanabe T and Sakai J 2012 Stress-induced VO_2 films with M2 monoclinic phase stable at room temperature grown by inductively coupled plasma-assisted reactive sputtering *Journal of Applied Physics* **111** 073514.

[51] Luo Y Y, Zhu L Q, Zhang Y X, Pan S S, Xu S C, Liu M and Li G H 2013 Optimization of micronano-structure and optical properties of VO_2 thin film prepared by reactive sputtering *Journal of Applied Physics* **113** 183520.

[52] Anders A 2005 *Surf. Coatings Technol.* **200** 1893-1906.

[53] Nag J 2011 *The solid-solid phase transition in vanadium dioxide thin films: synthesis, physics and application* (Doctoral dissertation) Nashville, Tennessee 41.

[54] Robbie K and Brett M J 1997 *J. Vac. Sci. Technol. A* **15** 1460.

[55] Robbie K, Sit J C and Brett M J 1998 Advanced techniques for glancing angle deposition *Journal of Vacuum Science & Technology B* **16(3)** 1115-1122.

[56] Nieuwenhuizen J M and Haanstra H B 1966 *Philips Tech. Rev.* **27** 87.

[57] Tait R N, Smy T and Brett M J 1993 Modelling and characterization of columnar growth in evaporated films *Thin Solid Films* **226** 196.

[58] Besnard A 2010 *Relations nano-structure-conductivité électrique dans des films de chrome architecturés* (Doctoral dissertation) Besançon.

[59] Dolatshahi-Pirouz A, Sutherland D S, Foss M and Besenbacher F 2011 Growth characteristics of inclined columns produced by Glancing Angle Deposition (GLAD) and colloidal lithography *Applied Surface Science* **257(6)** 2226-2230.

[60] Fujiwara H, Hara K, Kamiya M, Hashimoto T and Okamoto K 1988 *Thin Solid Films* **163** 397.

[61] Okamoto K, Hashimoto T, Hara K, Kamiya M and Fujiwara H 1985 *Thin Solid Films* **129** 299.

[62] Pandya D K, Rastogi A C and Chopra K L 1975 *J. Appl. Phys.* **46** 2966.

[63] Beydaghyan G, Buzea C, Cui Y, Elliott C and Robbie K 2005 *Appl. Phys. Lett.* **85** 153103.

[64] Kuwahara K and Shinzato S 1988 *Thin Solid Films* **164** 164.

[65] Deniz D, Frankel D J and Lad R J 2010 *Thin Solid Films* **518** 4095.

[66] Wang S, Xia G, He H, Yi K, Shao J and Fan Z 2007 *J. Alloy Comp.* **431** 287.

[67] Wang S, Xia G, Fu X, He H, Shao J and Fan Z 2007 *Thin Solid Films* **515** 3352.

[68] Lintymer J, Martin N, Chappé J-M, Delobelle P and Takadoum J 2005 *Surf. Coat. Technol.* **503** 177.

[69] Robbie K 1998 *Glancing Angle Deposition* (Doctoral Dissertation) University of Alberta, Canada.

[70] Jen Y-J, Lin M-J and Chao J-H 2010 *Sensors and Actuators B: Chemical* **149** 67.

[71] Wong M-S, Lee M-F, Chen C-L and Huang C-H 2010 *Thin Solid Films*.

[72] Yang H-Y, Lee M-F, Huang C-H, Lo Y-S, Chen Y-J and Wong M-S 2009 *Thin Solid Films* **518** 1590.

[73] Wang S, Fu X, Xia G and Wang J 2006 *Appl. Surf. Sci.* **252** 8734.

[74] Allouach H and Mankey G J 2005 *Thin Solid Films* **305** 1.

[75] Karabacak T, Mallikarjunan A, Singh J P, Ye D, Wang G C and Lu T M *2003 Appl. Phys. Lett.* **83** 3096.

[76] Seto M W, Dick B and Brett M J 2001 *J. Micromech. Microeng.* **11** 582.

[77] Lintymer J, Martin N, Chappé J-M, Takadoum J and Delobelle P 2006 *Thin Solid Films* **164** 164.

[78] Young N O and Kowal J 1959 *Nature* **183** 104.

[79] Kuwahara K and Hirota H 1974 *Jpn. J. Appl. Phys.* **13** 1093.

[80] Vick D and Brett M J 2006 *J. Vac. Sci. Technol. A* **24** 1331.

[81] Lintymer J, Gavoille J, Martin N and Takadoum J 2003 *Surf. Coat. Technol.* **181** 316.

3. Methodology

In this work we will present a method to create thin films of vanadium dioxide by physical vapour deposition. These films will have inclined columns, zig-zags and spiral nano-structures. In this chapter we will start by describing the general method to create thin films by DC magnetron sputtering, then, we will describe separately the methods to create the three nano-architectures above mentioned. We will end with the films produced with reactive sputtering by using oxygen during the deposition.

After the manufacturing of the films, these will be tested by running several experiments to discover which ones and with which parameters are better for obtaining vanadium dioxide. The methodology of these experiments is briefly explained.

Finally, the most suitable films are evaluated as captors for ozone gas sensing. The method employed for this is also described.

3.1 Film deposition

Firstly, Vanadium thin films were deposited on glass and silicon substrates by DC magnetron sputtering from a vanadium metallic target (purity 99.5 %), after cleaning them in acetone and alcohol.

The metallic target was sputtered with a constant current density J_{Va} = 100 $A.m^{-2}$ in argon atmosphere. The substrates were grounded and kept at room temperature and the chamber was pumped down to 10^{-5} Pa. The Argon mass flow rate was set constant in order to reach a sputtering pressure of 0.3 Pa (pumping speed was maintained at S = 13 $L.s^{-1}$). The deposition time was adjusted in order to deposit a constant thickness close to 400 nm for all films, later checked by profilometry.

Films with different vanadium nano-structures were created. The oxidized phases were reached by a subsequent thermal annealing treatment. Several experiments were then carried out to

characterize the films be studying the crystallographic nano-structure, the phase appearance, the morphology of the nano-structures and electrical conductivity of the films deposited. Finally, the most suitable films for gas sensing were elected and tests were carried out for ozone.

In the following subsections, each part of the methodology is explained in further detail.

3.1.1 Preparing the substrates

Keeping the substrate clean is very important for the quality of the film. Particles on it produce unwished roughness and a bad formation of the nano-architecture looked for. Specks make a shadowing effect on inclined columns much higher than the natural phenomena, sometimes even destroying the sample [1]. For this reason, the substrates employed in this work were carefully managed with forceps and special paper, never being touched with bare skin. They were then thoroughly cleaned with ethanol and acetone, polished with a high pressure air pistol and kept on boxes until needed.

Two different materials for the substrates were used: Glass and silicon. Glass allowed measuring the thickness of the film on it and testing the electrical resistivity, as glass does not compromise the validity of these results. Silicon on the other hand, allows the realisation of SEM (Scanning Electron Microscopy), XRD (X-ray Diffraction) and XPS (X-ray Photoelectron Spectroscopy) analysis.

The pieces of substrates were neatly cut with a diamond pointed pen. The dimensions were as illustrated in figure 3.1. When set on the substrate holder, before introducing them inside the sputtering machine, two thin lines are marked with an OH pen on each short side of the film. After the deposition, these lines are easily removed with alcohol and will later allow us to measure the film’s width easily with a profilometer.

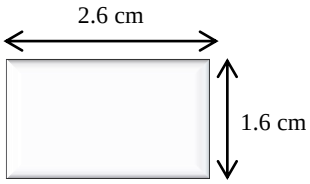

Figure 3.1: Dimensions of the substrates employed.

As silicon's width is approximately half of the glasses, an additional piece of silicon was inserted under the silicon used as substrate, so that both widths were equal during the deposition.

3.1.2 Deposition with the GLAD method

The DC magnetron sputtering machine employed is a home-made device developed in FEMTO-ST (Franche-Comté Electronique Mécanique Thermique et Optique - Sciences et Technologies) research institution, within the MN2S (Micro Nano Sciences and Systèmes) department and under the leadership of Nicolas Martin. This machine allows the technique GLAD to be employed successfully. Figure 3.2 is a picture of the device and its main parts. In figure 3.3 a scheme represents the machine for a better understanding of the system.

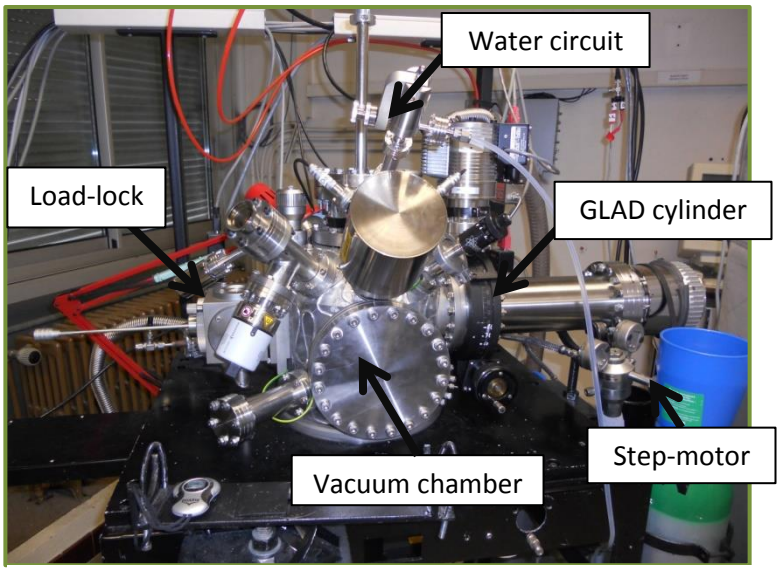

Figure 3.2: Picture of the home-made system used for GLAD deposition.

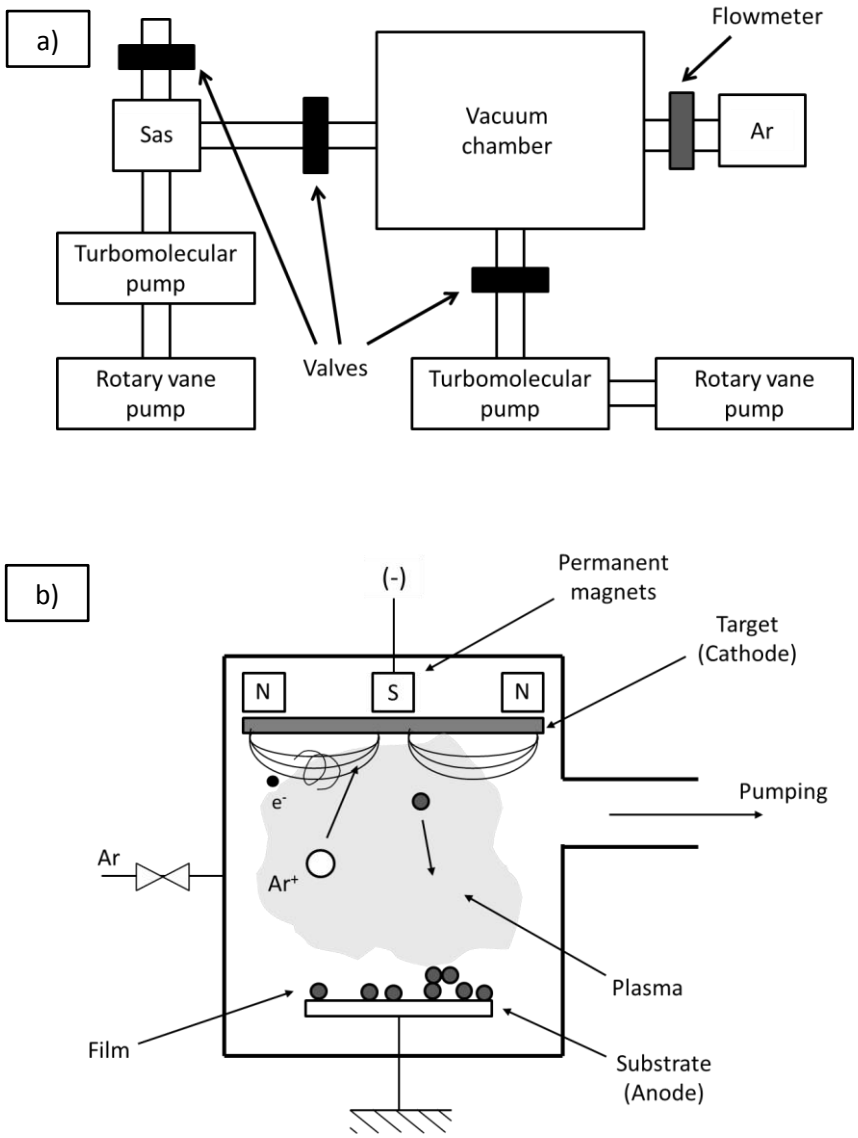

Figure 3.3: a) Scheme of the sputtering machine and b) detailed scheme on the sputtering principle.

In figure 3.3 a) we can observe a basic scheme on the sputtering machine. In figure 3.3 b) the vacuum chamber, where the deposition takes place, is seen in detail. Working in vacuum is essential. The vacuum chamber allows a good control on the composition and growth of the films. For this reason, an important pumping system is installed (pumping speed was maintained at S = 13 $L \cdot s^{-1}$). The value of the pressure achieved depends on the pumping power and the unavoidable leaks. To work at a given pressure, inert or reactive gases are injected into the chamber. The residual pressure achieved in the vacuum chamber was of 10^{-7} mbar, situated in the secondary vacuum (10^{-3}-10^{-8} mbar).

The correspondence between the most used pressure unities is:

$$760\ Torr = 1{,}01325\ 10^5\ Pa = 1{,}01325\ bar$$

To create the plasma, we first introduce argon in the vacuum chamber by opening a valve that connects to an argon gas bottle, until the vacuum pressure is of the order of 10^{-2} mbar. This happens with approximately 55% of Argon flow (11 sccm). After, we open the worm drive system installed and introduce the substrate in the vacuum chamber. We then unscrew the substrate holder and remove it, closing the worm drive. When we have placed securely the substrate on its place inside the vacuum chamber, we can either leave it horizontal or rotate it α degrees (form 90 to -90) with a cylinder that allows us to incline it manually. Also, we can rotate it in the azimuthal direction enhancing the step motor attached to the device.

Once the substrate is situated in the wished angle, enhancing the DC generator we produce a difference of voltage in the target by introducing a constant current density J_{Va} = 100 $A.m^{-2}$ and producing an electrical discharge. Given that argon is a neutral gas, it does not react with the other materials. The positive argon ions (Ar^+) from plasma are attracted by the vanadium metallic target, which is negatively polarized, and the vanadium ions are displaced from the target and move towards the substrate. During deposition the pressure is increased to approximately $3 \cdot 10^{-3}$ mbar by reducing the flow of Argon to 6-8% (1,2-1,6 sccm depending on the use of oxygen). There is also an oxygen bottle available in the device. The introduction of oxygen during deposition allows reactive sputtering, with the formation of vanadium oxides on the substrate during deposition.

To increase the speed of the deposition, a magnetron device is used. It consists in adding to the electrical field a strong magnetic field (of the order of one hundred Gauss) created by permanent magnets. The electrons coil around the field lines and therefore increase meaningfully the electronic density in the proximity of the target's surface, attracting the Argon ions strongly.

Even though it increases the deposition speed, the wear of the target becomes heterogeneous, as it follows the magnets field lines. We can observe a strongly worn out interior ring when we remove the target. This way, we can only use around a 30% of the target before it is useless [2,3]. There are studies made on new magnetrons that use rotary non-centred magnets, reducing this way the

wear of the target [4]. The DC magnetron sputtering machine employed also has an ion bombarding device installed, although it won't be used for this study.

During the first five minutes of all the depositions made the shutter is always placed in between the substrate and the target. This is necessary due to the unavoidable formation of a thin oxide layer on the target's surface and possible impurities. Five minutes is enough for this layer to be removed. The substrate and the target were always kept at room temperature and a water cooling system was continually working during the depositions.

Having been explained the general process used for all the depositions made during this work, the method to produce each type of the nano-structures will be detailed.

a) Metallic and inclined columns

The first sample was prepared by conventional sputtering with a normal incident angle α of the sputtered particles (α=0º), obtaining a metallic vanadium film. Then, the GLAD method was used to produce oriented columnar nano-structures. The home-made GLAD substrate holder allows an orientation change of the incident angle of the particles flux α from 0 to 90°. This incident angle was taken between the normal of the substrate and the normal of the target (i.e. the main direction of the sputtered atoms flux). The following angles were used: 20, 40, 60, 70, 80 and 85 degrees. The deposition time was adjusted in order to deposit a constant thickness close to 400 nm, later checked by profilometry after deposition. To do this, the first samples were done with short sputtering times (Table 3.1) and their thickness was measured. A mean was made between both sides of the films, as when the incidence angle is not zero, one of the sides grows faster than the other.

Table 3.1: Sputtering rate of the films for several incidence angles.

Incidence angle(°)	Sputtering Time(min)	Height Side 1 (nm/hour)	Height Side 2 (nm/hour)	Mean (nm/hour)
0	20	482	482	482
20	30	370	415	392
40	30	322	443	382
60	30	202	356	279
80	30	145	166	155

The relation of the sputtering rate (nm/h) vs. the incidence angle α (º) was found (Figure 3.4), so that the next films were deposited during the necessary time to be 400nm thick. The deposition times are detailed in table 3.2.

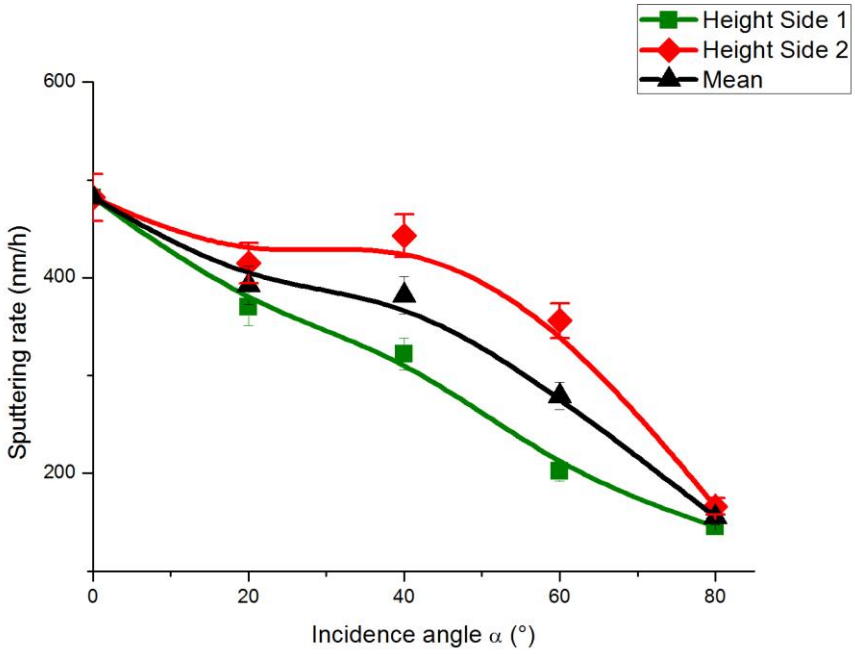

Figure 3.4: Sputtering rate dependence on the incidence angle α.

Table 3.2: Sputtering times needed to create 400nm thick films depending on the incidence angle.

Incidence angle(º)	Sputtering time for 400nm (min)
0	50
20	60
40	63
60	86
70	110
80	156
85	218

b) Zig-zags

To obtain zig-zag nano-structures, α=80º was set fix. The same method as in inclined columns was used, except the substrate was rotated with φ = 180º each time a change of orientation was desired. This way, for one zig-zag, the substrate was rotated only once at half the time of the deposition. For two zig-zags, the substrate was rotated three times. Seven times for four zig-zags and, finally, fifteen rotations for eight zig-zags.

c) Spirals

To obtain spiral nano-structures, the incidence angle α was also set fix for 80º and the angle φ had to be continually in rotation. To this aim, the step-motor was used with the parameters detailed in table 3.3. The rotation speed was determined by dividing the revolutions desired by the deposition time for α=80º (156 minutes). The time for each step (T) was obtained from (3). Films with approximately one spiral, two spirals, four spirals and eight spirals were produced.

Table 3.3: Step-motor parameters for each spiral nano-structure.

Number of spirals	*1*	*2*	*4*	*8*
Rotation speed (Rev.h-1)	0,3846	0,7692	1,538	3,077
T (s)	8,13	3,32	1,35	0,553

$$Log(RS_s) = -7.7351x10^{-1}\ x\ Log(T) + 6.6545x10^{-1} \quad \textbf{(3)}$$

3.1.3 Reactive sputtering combined with GLAD

It seems interesting to use oxygen during deposition, as the final aim is to obtain the phase VO_2. Therefore, an oxygen flow was injected to the plasma for several samples.

Films with a continuous flow of 1,3,5,8 and 10 % of oxygen were created. When measuring the resistivity on the films roughly, even the one with 1% was too resistive to measure with a common ohmmeter. The injection device used was unable to introduce a flow rate below 1%, so the solution was to insert pulses of oxygen instead, like the ones described in figure 3.5.

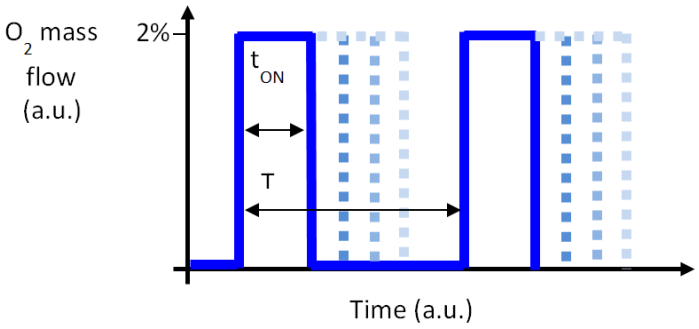

Figure 3.5: Scheme of the oxygen pulses employed.

Firstly, the pulses period had to be determined. A maximum flow rate of 2% was set and several periods were tried out. The maximum variation of voltage was measured and plotted for each period (Figure 3.6).

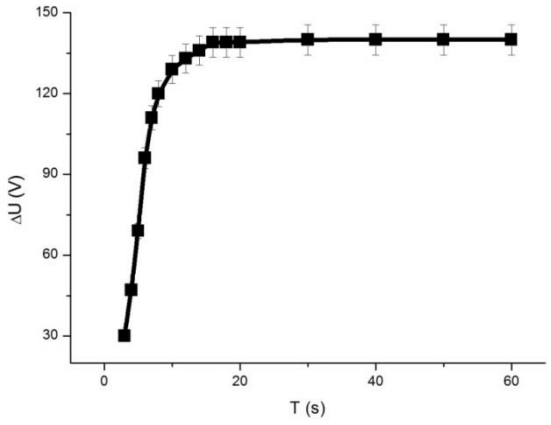

Figure 3.6: Maximum variation of voltage for different periods of oxygen injected.

It was concluded that a period of 16 seconds was the most appropriate. Once the period was determined, the injection time (T_{ON}) was shifted from 2 seconds to 12 seconds, obtaining the deposition rates illustrated in Figure 3.7.

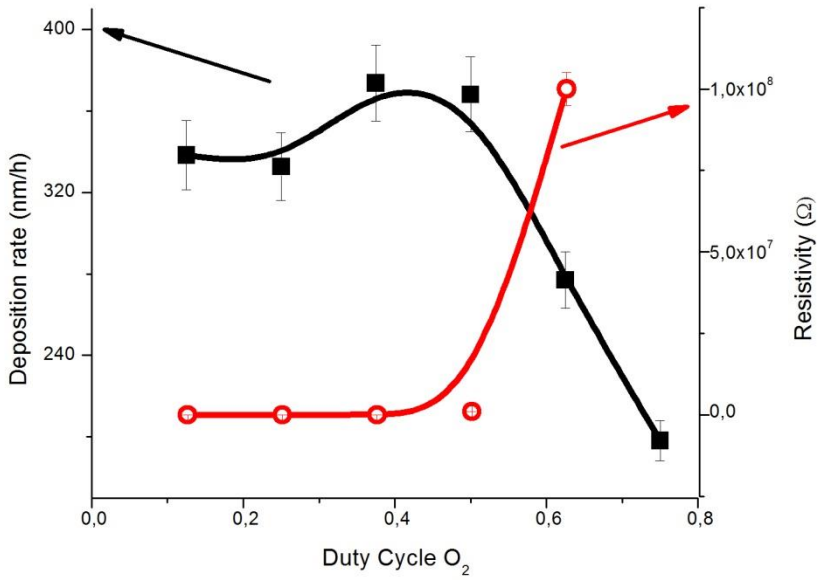

Figure 3.7: Deposition rate and resistivity in front of the oxygen pulses duty cycles tested.

For $t_{ON} \geq 8\,s$ the films were too resistive and therefore not interesting for obtaining VO_2. Samples with 2, 4, 6 and 8 seconds of oxygen injection were done, with a thickness of 400nm. In conclusion, the oxygen duty cycles dc (4) taken into account were: 0.125, 0.25, 0.375 and 0.5.

$$dc = \frac{t_{ON}}{T} \quad \textbf{(4)}$$

3.2 Annealing treatment and resistivity measurements

Both for the samples deposited by GLAD and for the ones deposited by GLAD and oxygen pulses, the oxidized phases were reached by a subsequent thermal annealing treatment of the vanadium films. These were heated in air using temperature 11 cycles from 30ºC up to 550ºC, starting at room temperature and going up to the desired temperature to then return to ambient temperature at 5 ºC min^{-1}, stabilising in each temperature for two minutes. In this way, a rigorous control of the vanadium

oxide phase's appearance in the films could be done. Each one of the cycles is described in table 3.4. The DC electrical conductivity of the films deposited on glass substrates was measured using a home-made device in the Van Der Pauw geometry [5] whilst being annealed, recording the resistivity in function of the temperature.

Table 3.4: Temperature cycles used to anneal the films.

Cycle number	**Temperature cycle (ºC)**
1	30-50-30
2	30-100-30
3	30-150-30
4	30-200-30
5	30-250-30
6	30-300-30
7	30-350-30
8	30-400-30
9	30-450-30
10	30-500-30
A	30-100-30
11	30-550-30
B	30-100-30

In addition, two more cycles (A and B) were done, before and after the eleventh cycle respectively. These two heating cycles allowed the study of the hysteresis loops observed at around 68ºC for VO_2.

3.3 Films characterization

In order to find the best conditions to create VO_2, the films were studied enhancing different techniques to evaluate the most significant properties to our work.

3.3.1 Scanning Electron Microscopy (SEM)

Firstly, the morphology was observed with SEM photographs to ensure the films created were achieving the nano-structures desired. Pictures of the 400nm thick films without oxygen pulses were made for: Inclined columns (0º, 70º, 80º and 85º), zig-zags (1, 2, 4 and 8 periods) and spirals (1, 2 and 8 turns).

3.3.2 DC-Resistivity

The films resistivity to electric current in function of temperature is what allows observing the change of phases from semi-conductor to metallic when having VO_2. Therefore, it is of extreme importance to control these parameters thoroughly. A home-made system (Figure 3.8) was used to this aim, consisting in four tips that measure the resistivity of a film in the Van der Pauw geometry at the same time that a heated cylinder anneals the film. The annealing cycles are controlled with LABVIEW software, which indicates the temperature and resistivity at every moment.

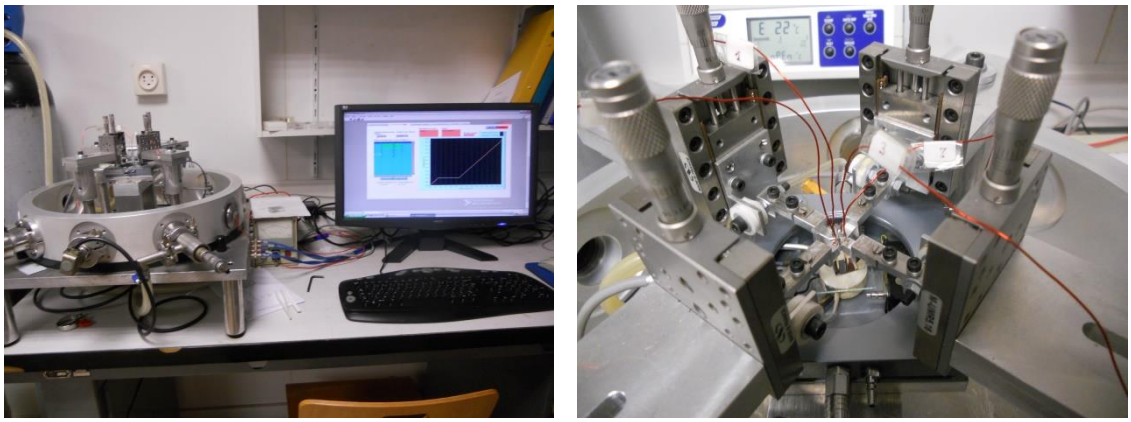

Figure 3.8: Pictures of the device used to anneal the vanadium films and record the DC-resistivity in function of the temperature.

3.4 Ozone sensing

Once all the significant studies were done, the most suitable films for sensor captors were tested. These were the films containing more VO_2 and with considerable resistivity ranges for gas sensors.

The used sensor was the *Multi-Sensor-Platform MSP 632* by *Heraeus* (Figure 3.9). The exterior legs are connected to a heater and the interior legs are connected to resistances to measure the resistivity. Vanadium was deposited on it with the parameters chosen, protecting the sensor's legs from the sputtering by covering them up with a piece of glass. After, the sensor was annealed on the DC-resistivity device.

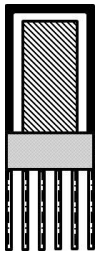

Figure 3.9: Scheme of the Multi-Sensor-Platform MSP 632 by Heraeus.

With the help from the research institution *Chrono-environnement* attached to the University of Franche-Comté (UFC), the sensors were tested as ozone gas captors with the system

shown in figure 3.10. The scheme, also in figure 3.10, represents the operating method of the system. Dry air is injected to a UV generator lamp that produces ozone (O_3). The film, deposited on the sensor cell, receives the ozone and reacts, experiencing a change in its resistivity. Ozone is an oxidizing gas, thus, it gathers electrons from the vanadium oxides film's surface. The films are n-type semi-conductors, so consequently the resistivity increases when injecting ozone.

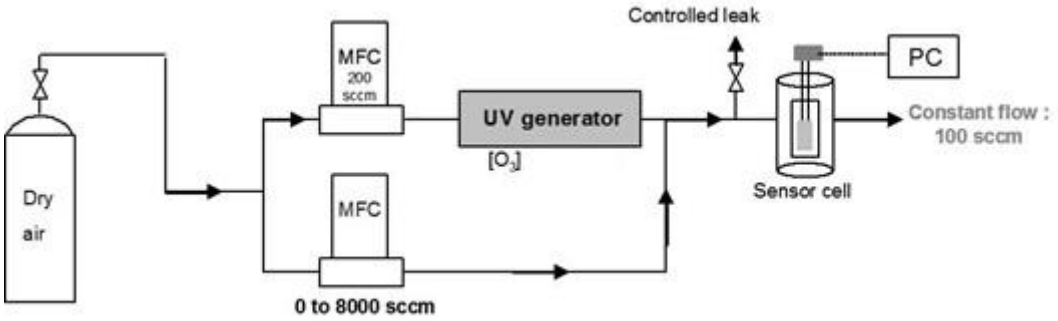

Figure 3.10: Picture and scheme of the ozone generator and sensor cell devices used at Chrono-environnement.

Temperature was varied to obtain the resistivity changes at different temperatures and, therefore, find the optimal functional point of the sensor; the one representing a bigger variation of resistivity when injecting ozone. Also, after using only dry air, slight values of humidity were added.

Bibliography of chapter 3

[1] Richardt A and Durand A-M 1994 *Le vide, les couches minces, les couches dures* Editions In Fine Paris.

[2] Swann S 1988 *Vacuum* **38** 791.

[3] Fan Q H and Chen H Y 1993 *Thin Solid Films* **229** 145.

[4] Iseki T, Maeda H and Itoh T 2008 *Vacuum* **82** 1162.

[5] Besnard A 2010 *Relations nano-structure-conductivité électrique dans des films de chrome architecturés* (Doctoral dissertation) Besançon 77.

4. Results and interpretation

4.1 GLAD Results

4.1.1 Inclined columns

The first films created were the ones using GLAD with different angles of inclination. These films were studied carefully to find the one with better properties for gas sensing.

a) Morphology

The morphology of the nano-structures was verified by scanning electron microscopy (SEM) observations on the fractured cross-section of the films deposited on silicon substrates.

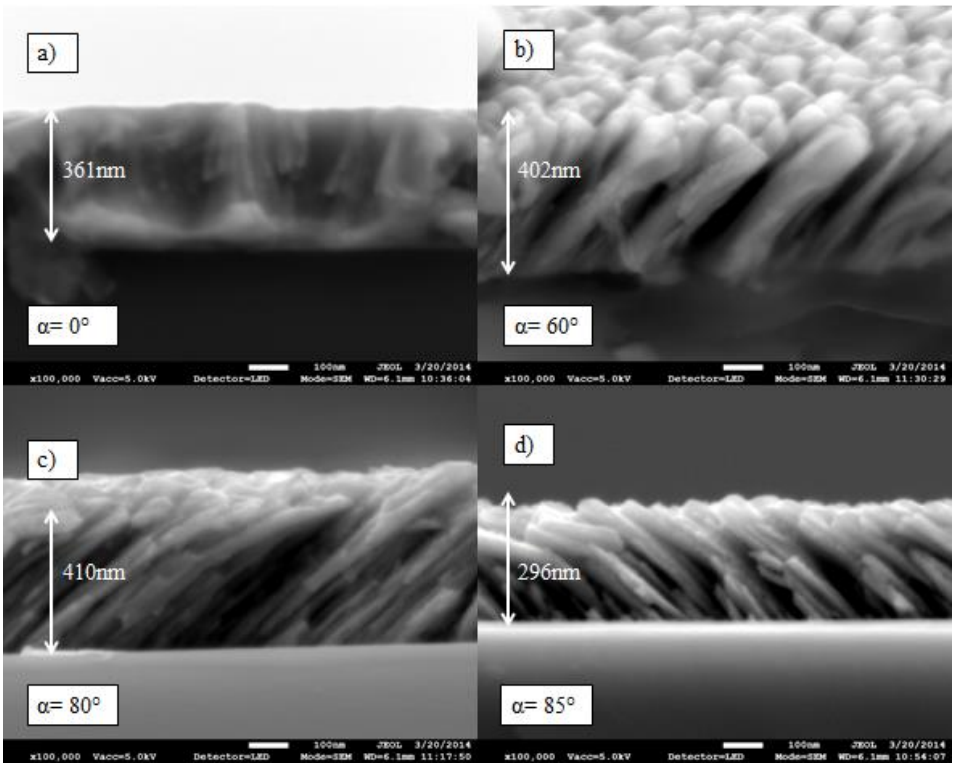

Figure 4.1: X10000 SEM images of the cross section of thin vanadium films with sputtering incidence angles α equal to 0º, 60º, 80º and 85º respectively.

In Figure 4.1, the SEM images of the thin vanadium films show the morfology of the cross section according to the angle of incidence used during the sputtering process. An incident angle of $\alpha = 0^{o}$ showed a very dense and poorly defined column nano-structure (Figure 4.1 a)) , in agreement with Thornton [1], of dominating poorly oxidated V. When the incidence angle α increases, it leads to more defined and inclined columns ($\alpha = 60^{o}$, 80^{o} and 85^{o}, figure 4.1 b), c) and d), respectively). The black areas show a clear porous nano-structure that increases with α and leads to co-existing VOx phases, which is in agreement with previous investigations [2, 3a].

Porosity is related to the density of the film in function of the incidence angle. If a large columnar angle (more parallel to the substrate) is wanted, the incidence flux must be deposited at a large oblique angle, resulting in a very porous film. On the other hand, if a more vertical columnar film is desired, the flux must arrive more perpendicularly to the substrate. The resulting film will then have a tightly packed, dense nano-structure [4].

The scanning electron micro-graphs of vanadium films deposited at 0^{o}, 60^{o}, 80^{o} and 85^{o} shown in figure 4.1 were also used to roughly measure the column inclination angles β. The angles agree closely to Tait's relationship (Figure 4.2 a)), representing a much lower percentage of deviation than the tangent's rule towards the real measurements (Fig. 4.2 b)). The measured column inclination angles β are detailed in table 4.1, along with the column angles β predicted both by the tangents rule and Tait's rule.

Table 4.1: Comparison of the column angle β in function of the incidence angle α for the experimental value, tangent's rule and Tait's rule.

Incidence angle α (º)	**Column angle β (º)**	**Column angle β (º) according to the tangents rule**	**Column angle β (º) according to Tait's rule**
0	0 ± 1	0	0
60	44 ± 4	40,86	45,52
80	54 ± 4	70,57	55,6
85	46 ± 8	80,08	57,84

The column angle β increases with the incidence angle α, although a wrong tendency is observed in 85º, where β should increase respect 80º [4]. However, the accuracy of this last measurement is highly vague, having been estimated a deviation of ± 8º.

In figure 4.2 a), the relationship between the incident flux angle α and the columnar growth angle β is described for a fixed set of deposition conditions (material, gas composition and pressure, temperature and vapor energetics), both by the tangent's rule and Tait's rule. The experimental data obtained is also plotted. In figure 4.2 b) it is observed that Tait's deviation respect the experimental data obtained is lower than the tangent's. Thus, we can conclude Tait's rule is more accurate.

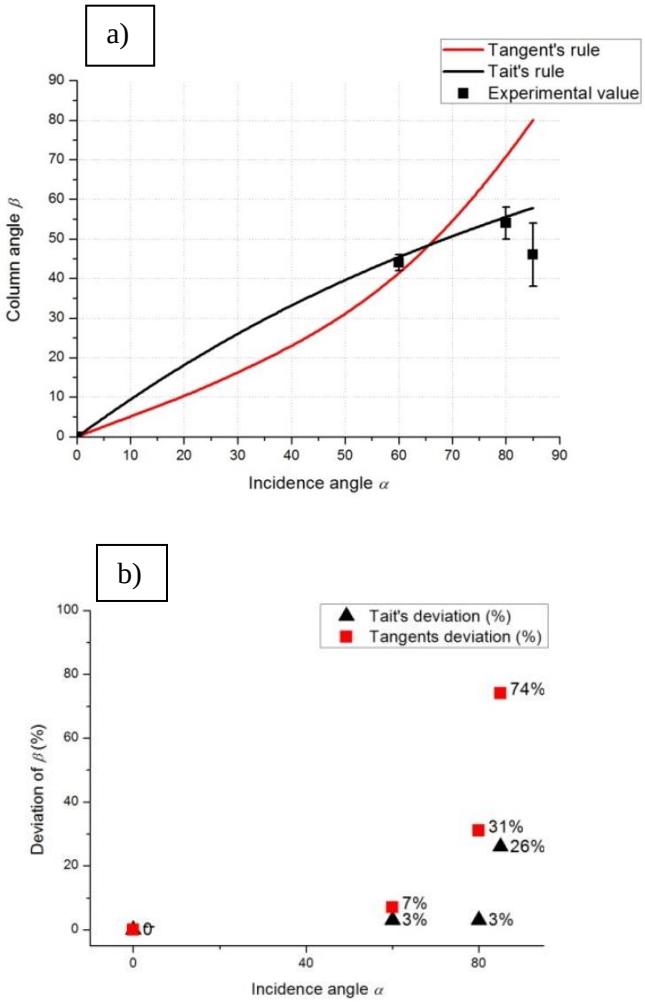

Figure 4.2: (a) The black line represents the tangent rule and the red line Tait's rule. The black dots are the experimental values obtained with SEM microscopy. (b) Percentage deviation (5) of each fixed relationship in front of the experimental values.

$$\%Deviation = \frac{Experimental\ \beta - Theoretical\ \beta}{Experimental\ \beta} \quad \textbf{(5)}$$

The discrepances between the experimental values of β and those proposed by the tangent rule are most certainly to be attributed to the shadowing effect [5,6]. Peaks of the surface undulation are exposed to incoming particles from all directions and thus grow faster than the average growth rate. At the same time, valleys of the surface undulation receive fewer particles since they are screened by peaks; therefore, their growth lags behind. This leads to inestability of the planar surface and results in the development of a columnar nano-structure [7]. It is also attributed to the mean free path of the

sputtered particles, which is lower than the target-to-substrate distance. This fact induces to a dispersion of the sputtered particles.

In the SEM images we can also observe a perpendicular growth during the first growing stages, before the shadowing effect is noticeable, which is in agreement with previous research [3C, 4 and 8].

b) DC-Resistivity

The electrical resistivity (ρ) of the films, at a fixed temperature of 30ºC, increases with the incidence angle α (Figure 4.3). The increase of the potential barrier is due to the gain in porosity of the columns [9]. In the same figure it is also represented the Temperature Coefficient of Resistivity (TCR) (5) in front of the incidence angle at 30ºC.

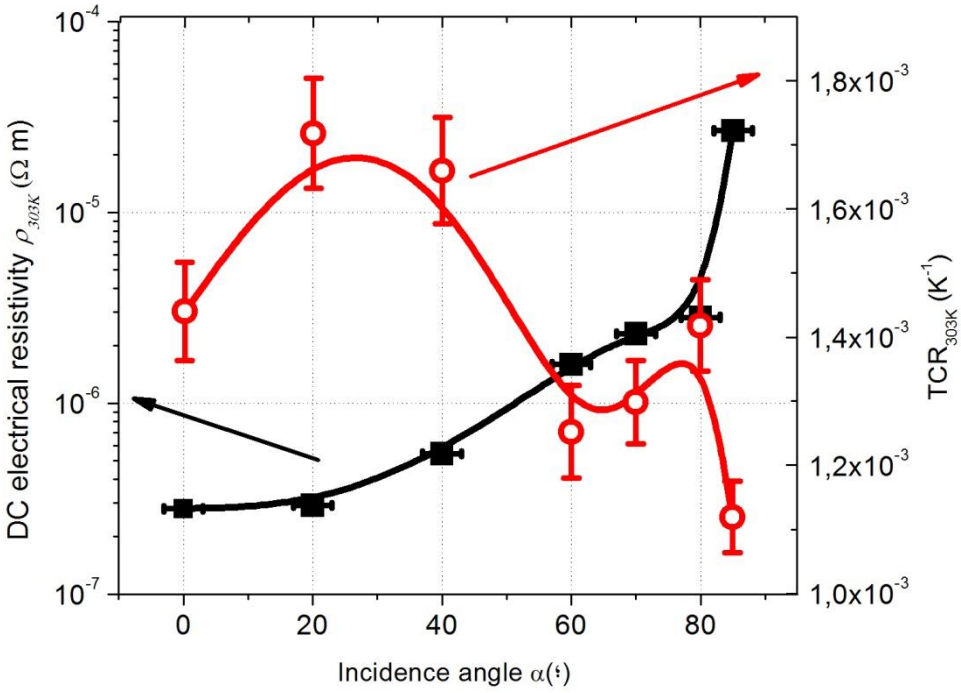

Figure 4.3: Electrical resistivity and temperature coefficient of resistivity for every incidence angle at 30ºC.

Bulk Vanadium has a fixed resistivity of 2,02·10-7 Ω·m at 27ºC [10], very similar to the one obtained experimentally for $\alpha = 0^0$. In the sputtering process the TCR (5) increases during the lowest incidence angles until it reaches a maximum value in between 20º and 30º. After this, it decreases

sharply and continually. This can be explained by the obtainance of a more porous nano-structure of the film with a higher incidence angle, being vanadium oxides less conductive that vanadium itself.

$$TCR = \frac{1}{\rho}\frac{\partial \rho}{\partial T} \quad \textbf{(5)}$$

In figure 4.4 the experimental curves of resistivity in front of temperature for every cycle were ploted for the following incidence angles: 0º,60º,70º and 85º. 11 heating cycles were employed in each film, previously described in table 3.3.

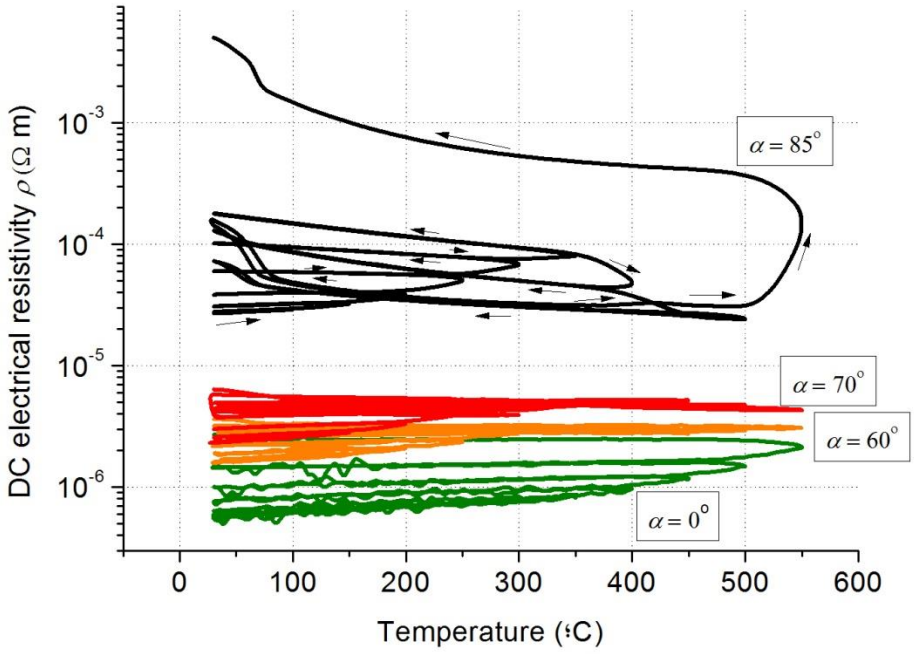

Figure 4.4: Electrical resistivity in front of the eleven temperature cycles (table 3.3) for incidence angles: 0, 60, 70 and 85º.

From the results, we can conclude that when we increase the incidence angle α we increase the resistivity of the film. This is in accordance with the increase of porosity and, therefore, oxygen content. Also, we observe how resistivity increases with temperature in every cycle for 0º and 60º, as it is expected due to the semi-conductor behaviour of the films being annealed. Nevertheless, after cycle seven (350ºC-400ºC), in 60º we start to notice how the resistivity slope changes tendency and becomes stable instead of increasing, even showing a slight drop. In 70º the tendency is confirmed; resistivity starts to fall clearly towards the seventh cycle. In the 85º film the drop is dramatically observed:

during cycles eight and nine the resistivity decreases when the film is heated (figure 4.5). In the tenth cycle we see the expected hysteresis cycle between 30ºC and 100ºC due to the formation of VO_2 phase. Finally, the film is annealed in the eleventh cycle and the resistivity increases in almost two orders of magnitude.

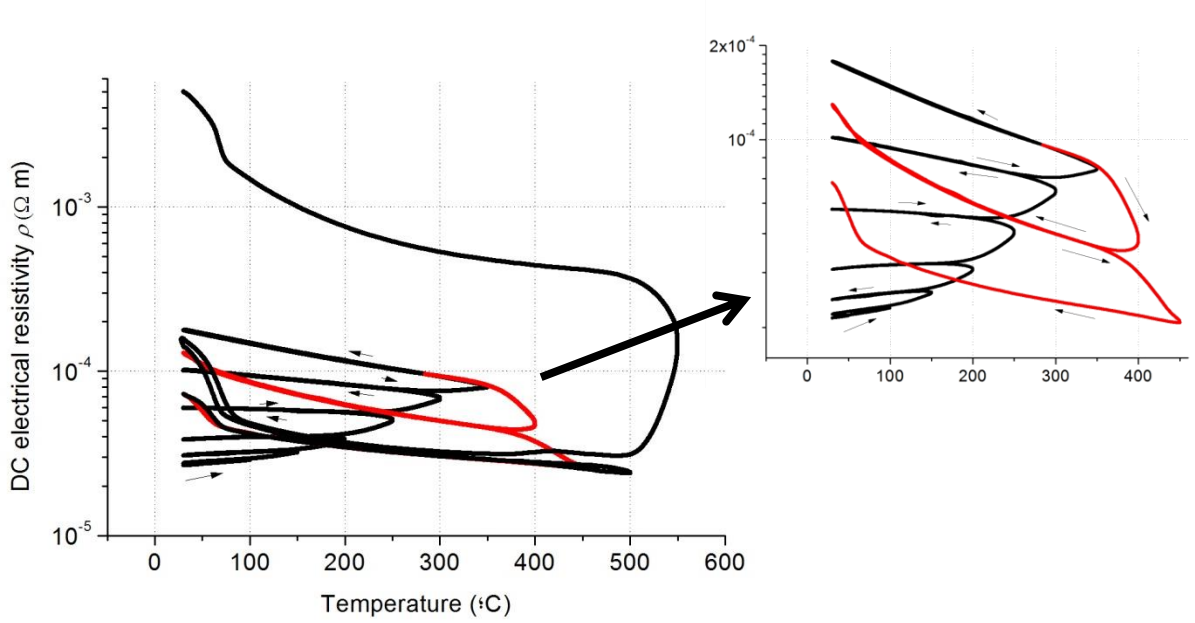

Figure 4.5: Electrical resistivity in front of the eleven temperature cycles for the GLAD film with incidence angle $\boldsymbol{\alpha = 85^0}$.

In red, zoom of the drop of resistivity during cycles eight and nine.

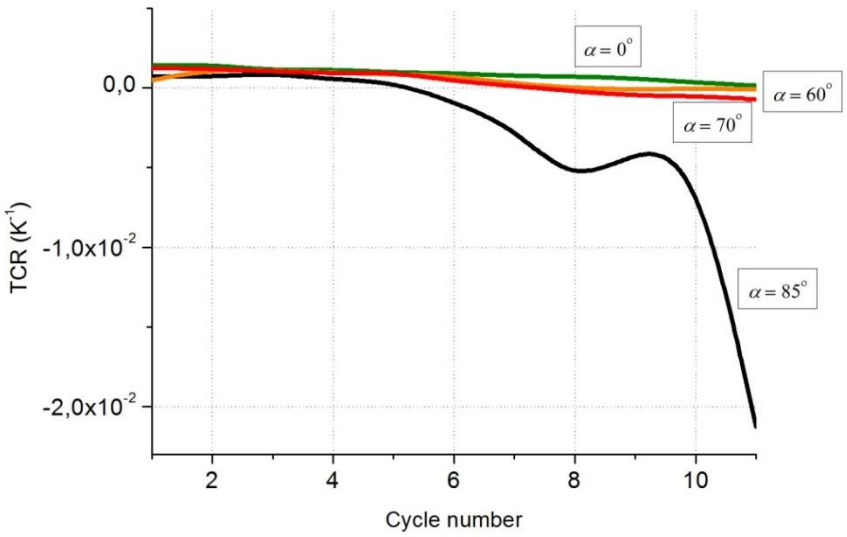

Figure 4.6: TCR in front of the heating cycles for the incidence angles 0, 60, 70 and 85º.

When plotting the TCR in front of the cycle number for these angles, we state the fact that after 60º the TCR becomes clearly negative (figure 4.6). This phenomenon may be explained by studying the different vanadium oxides produced within the annealing. As explained in section 2.1, in addition to vanadium dioxide (VO_2), vanadium sesquioxide (V_2O_3) and vanadium pentoxide (V_2O_5) there are nearly twenty other stable oxide phases (figure 2.2) whose phase diagrams are similar to those of VO_2 and V_2O_3, creating a special difficulty in growing thin films of VO_2. All of these phases, except one, exhibit a change from metallic to semi-conductor transition. V_7O_{13} is the only vanadium oxide which is always metallic. This is why the resistance starts to fall with temperature, as the metallic behaviour of V_7O_{13} makes its presence. In figure 4.7, a brief scheme of the appearance of vanadium oxides during the heating cycles is represented.

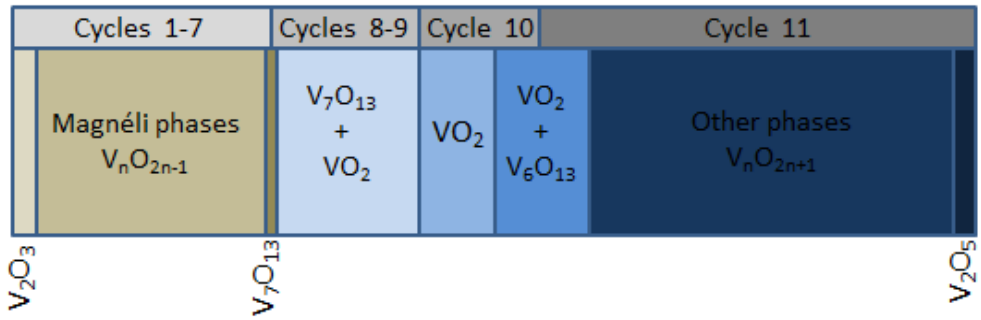

Figure 4.7: Proposal of vanadium oxides phase appearance during annealing.

If after the eleventh cycle we heat the films to 100ºC (cycle B), we are able to observe the characteristic VO_2 hysteresis loop in all of the angles, being more significant with the more oblique ones, specially 85º (figure 4.8.). The large change in resistivity during the semiconductor-to-metal transition for VO_2 occurs at Tc close to 68ºC (figure 4.9) in agreement with many references [11,12 and 13]. This will be useful for gas sensor applications, given the change in resistivity of the film.

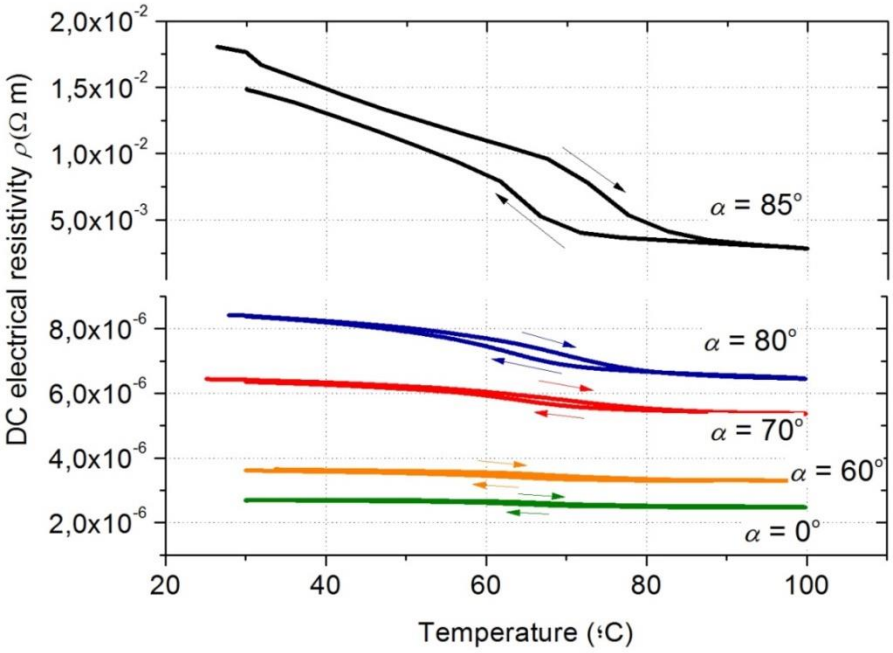

Figure 4.8: Hysteresis curves showing the change in resistivity as a function of temperature during phase transition in VO_2.

By shifting the film's temperature close to the metal-insulator interval, the conductance of the film becomes remarkably responsive to slight changes in molecular composition, pressure, and temperature of the gas environment [51], which is why it is useful for gas captor's applications.

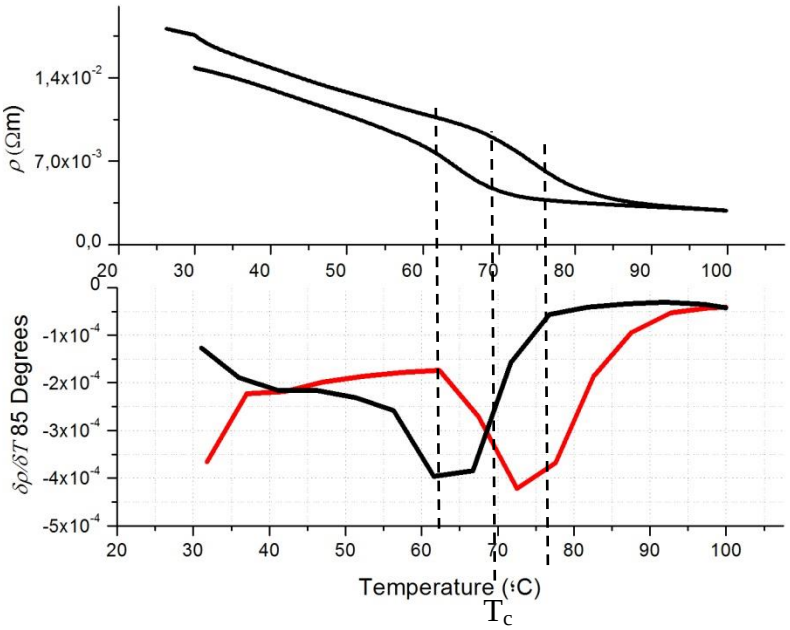

Figure 4.9: Hysteresis loop of the film deposited at 85 degrees. dρ/dT exhibits two peaks; the distance between them is taken as the width of the loop ΔTc = 14ºC ; the midpoint between the peaks is Tc=69ºC.

c) Chemical composition

It can be deduced that the film containing more VO_2 phase is the one with an incidence angle $\alpha = 85^0$ due to its hysteresis loop from 30 to 100ºC. Nevertheless, to scientifically prove the existence of this phase other experiments are needed. XPS and Raman Spectroscopy should be used to determine the phase's occurrence in the films. Tests were carried out for incidence angles 0,60,70,80 and 85º in different states. Firstly, in their metallic state (no annealing treatment), secondly, annealed to 350 ºC and finally, to 550ºC.

However, the device employed in FEMTO-ST has a low sensibility for measurements and vanadium oxides distinguish themselves with around this same sensibility. Thus, it is impossible to distinguish the vanadium oxides present in the films. Instead, what can be measured is the percentage of oxygen and vanadium present. Due to lack of time, the results could not be analysed. For the future work, the results of XPS must be analysed and Raman Spectroscopy should be used to back-up these results.

d) Crystallography

The crystallographic nano-structure was investigated by XRD using monochromatic Co K_α radiation with a Bragg-Brentano configuration θ/2θ. The Debye-Scherrer method was used to calculate the crystallite grain size. Unfortunately, due to lack of time these results could not be analysed.

4.1.2 Zig-zags

Zig-zag nano-structures were created with approximately one, two, four and eight orientation changes (zig-zags), with an incidence angle of 80º. Both the morphology studies and DC-resistivity measurements were done in the same way as the ones with inclined columns.

a) Morphology

The morphology of the nano-structures was also verified by scanning electron microscopy (SEM). In figure 4.10, the SEM images show the zig-zag nano-stractures obtained for an incident

angle of α = 80º with different number of zig-zags. After four zig-zags, the nano-structure starts to create undefined nano-structures.

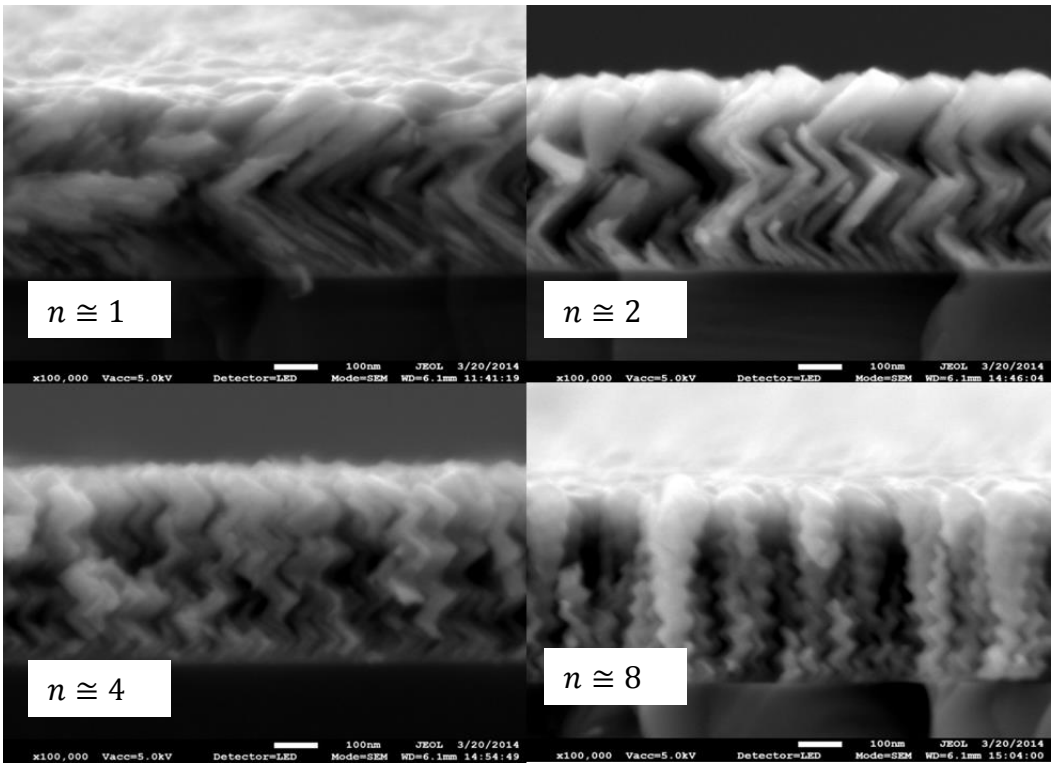

Figure 4.10: X100.000 SEM images of the cross section of thin vanadium films with a sputtering incidence angle α equal to 80º and approximately 1,2,4 and 8 zig zags respectively.

b) DC-Resistivity

When studying the resistivity in front of temperature for all the zig-zag nano-structures, the behaviour is the same than for inclined columns, except that in the last cycles the resistivity does not increase as much. The hysteresis loops obtained are vaguer and less meaningful than the one for an inclined column with α = 80º, as shown in figure 4.11. Also, a minimum resistivity is needed for gas sensing, and the resistivity measured for zig-zags is very low, meaning the films are more metallic. For these reasons, it is concluded that zig-zag nano-structures are not as good for gas sensing and no more experiments are needed for these films.

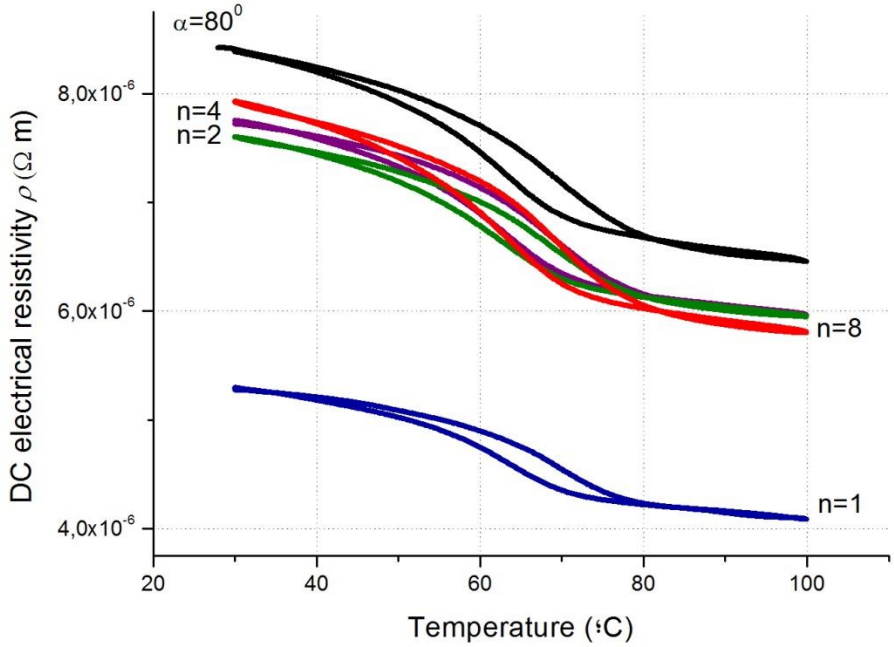

Figure 4.11: Hysteresis loops for all zig-zag nano-structures in comparison to inclined columns with α=80º.

4.1.3 Spirals

Spirals nano-structures were created with approximately one, two, four and eight periods, with an incidence angle of 80º. The morphology studies and DC-resistivity measurements were done in the same way as the ones with inclined columns and zig-zags.

a) Morphology

The morphology of the spirals nano-structures was also verified with SEM. In figure 4.12, the SEM images show the spirals obtained for an incident angle of α = 80º and different periods. After four spirals, the azhimutal angle φ rotation is too fast to create defined spirals, giving place to a tubular nano-structure.

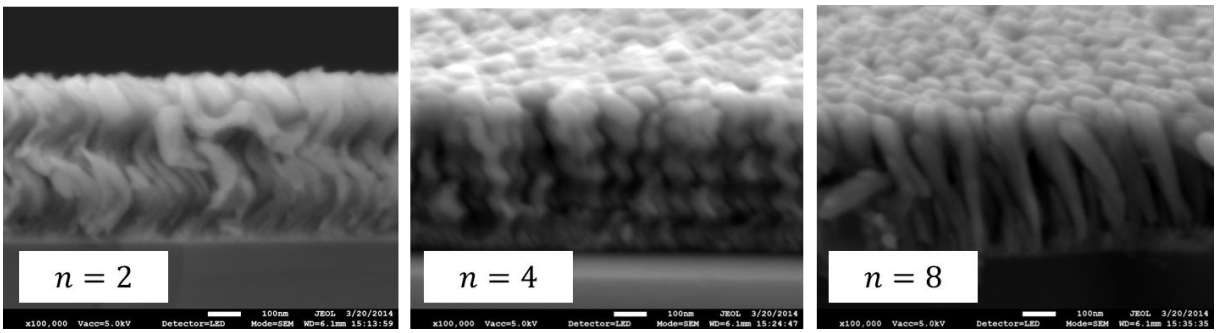

Figure 4.12: X100.000 SEM images of the cross section of thin vanadium films with a sputtering incidence angle α equal to 80º and approximately two, four and eight spirals respectively.

b) DC-Resistivity

When studying the resistivity in front of temperature for the spiral nano-structures, the behaviour is the same that for zig-zags: The hysteresis loops obtained are vaguer and less meaningful than the one for an inclined column with α = 80º, as shown in figure 4.13. Also, as explained previously, a minimum resistivity is needed for gas sensing and the resistivity measured is too low. Therefore, it is concluded that spiral nano-structures are not as good as inclined columns for gas sensing and no more experiments are needed for these films.

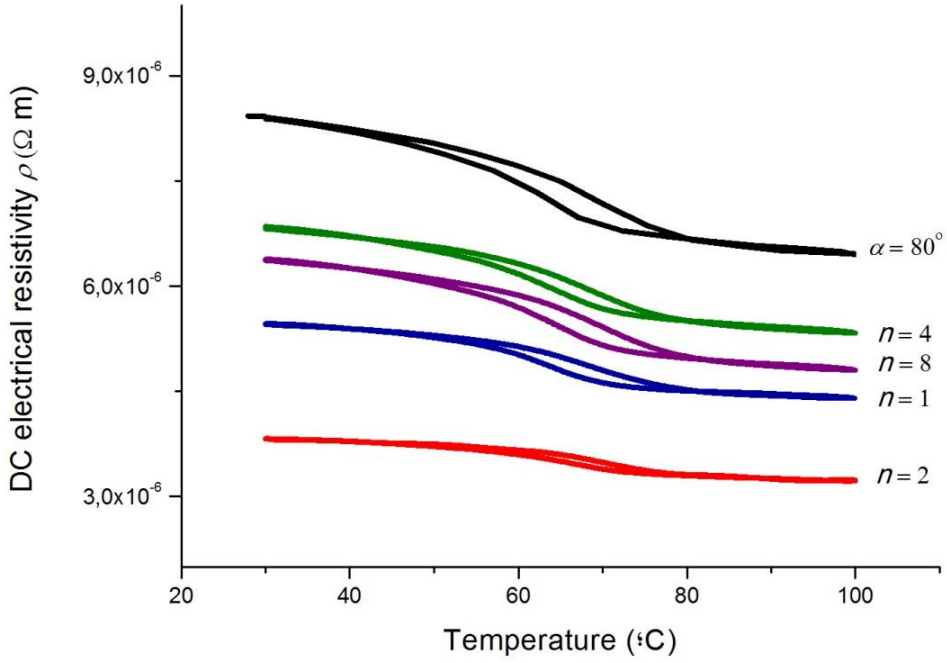

Figure 4.13: Hysteresis loops for all spirals nano-structures in comparison to inclined columns with α=80º.

4.2 Conclusions on GLAD Results

Having studied the three different GLAD deposited nano-structures; Inclined columns, zig-zags and spirals, it is concluded that inclined columns with incidence angle α = 85º are the most suitable films to obtain VO_2. This conclusion is supported with the wide hysteresis loops obtained, both before and after annealing the film to 550ºC, for temperatures in between 30 and 100ºC. Also, the resistivity values are higher than for the other nano-structures due to a higher porosity, being this property crucial for gas sensing applications. In figure 4.14 the best hysteresis loop for GLAD is plotted and the higher and lowest resistivity values indicated. The film with the biggest width (resistivity variation) is the most suitable film for captors.

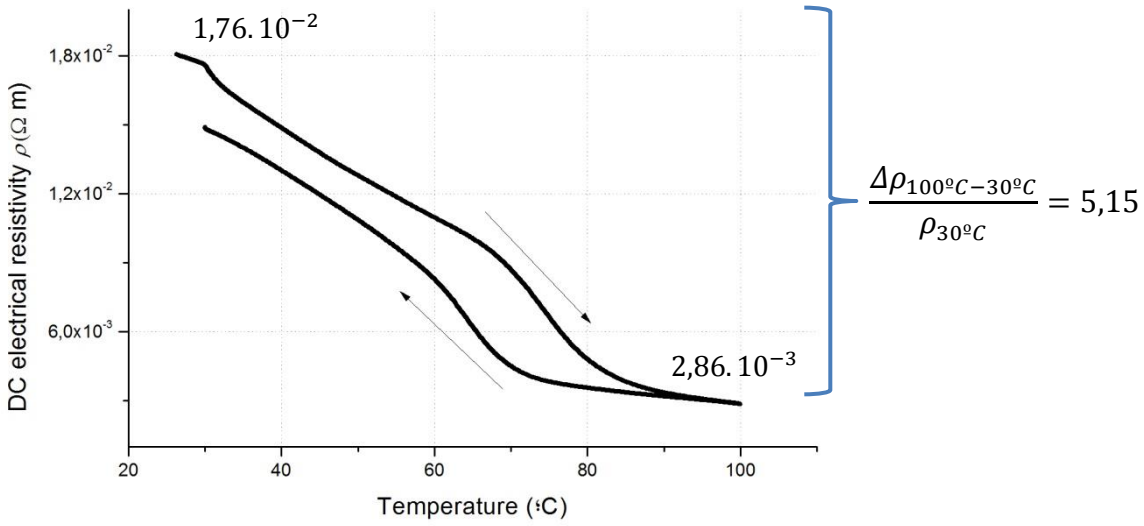

Figure 4.14: Hysteresis loop for α=85° heating from room temperature to 100ºC, after having annealed the film to 550ºC. The maximum and minimum resistivity measurements are indicated, as well as the resistivity variation.

4.3 GLAD + Oxygen pulses results

After depositing films with GLAD, it seems only logical to introduce oxygen into the vacuum chamber to study films oxidized during deposition. However, the flow of oxygen that can be introduced is limited, as if it is too high the resulting films will oxidize out of control and the VO_2

phase will not be achieved. An incidence angle of $\alpha = 85^{\circ}$ was used and rectangular oxygen pulses were introduced during deposition. The maximum flow was of 0,4 sccm, the period used was of 16 seconds and the duty cycles were the following: 0.125, 0.25 and 0.375.

The films obtained were studied in the same way as the GLAD films. The behaviour was very similar to inclined columns, specially the one with $\alpha = 85^{\circ}$. It was observed that for different amounts of oxygen the hysteresis loop before and after annealing to 550ºC was significantly different, being sometimes better before 550ºC (which never happened for inclined columns). The phase transition loops are detailed in figure 4.15, before and after annealing to 550ºC.

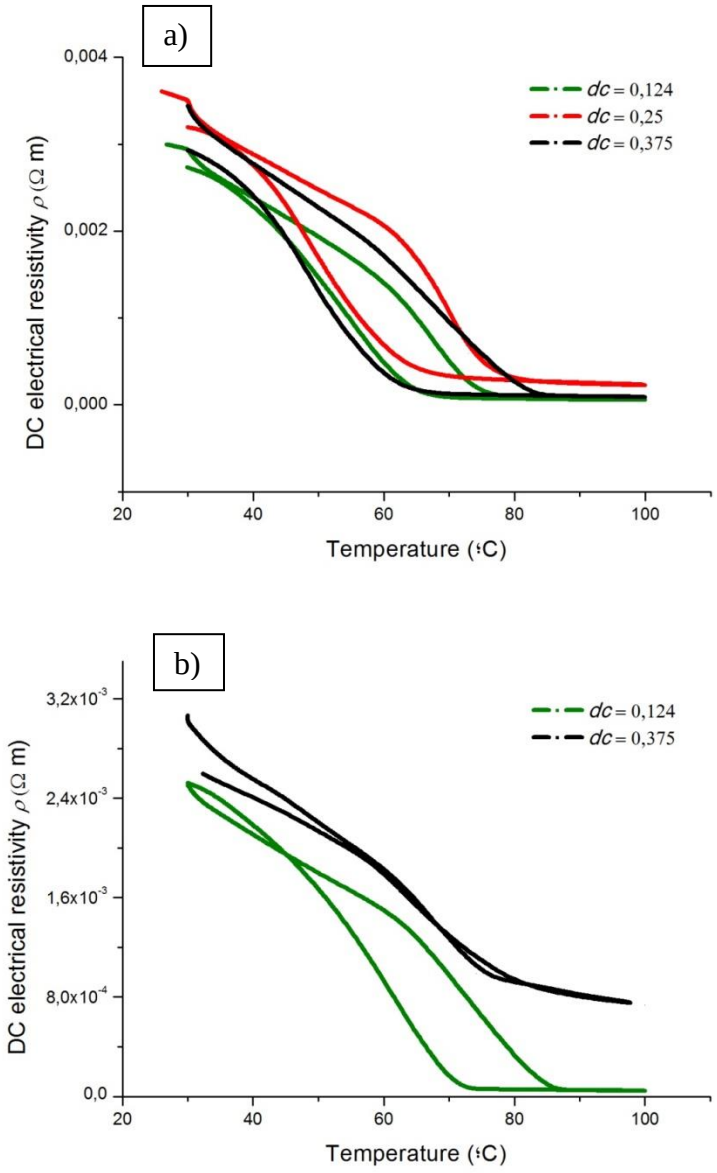

Figure 4.15: Hysteresis loops for the MIT transition of the films obtained by GLAD and oxygen pulse for each duty cycle used. Figure a) shows the loops for the films annealed to 500ºC and figure b) for the films annealed to 550ºC.

In figure 4.15 b), the loop for dc=0.25 is not taken into account due to the illogical values measured, probably for an error during the annealing treatment (the glass where the sample lied on broke during the heating process).

4.4 Conclusions on GLAD + Oxygen pulses results

When annealing to 500ºC, the film with a better hysteresis amplitude is the one with a dc=0,375, as can be seen in figure 4.16.

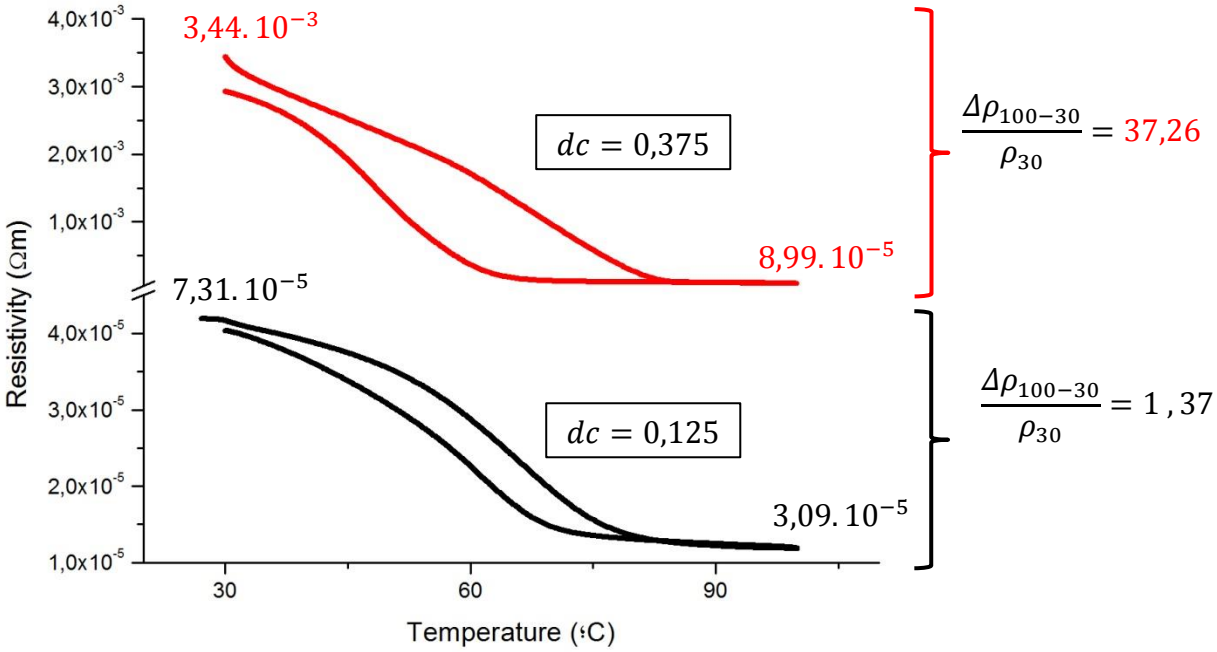

Figure 4.16: Hysteresis loops for dc=0,375 (in red) and for dc=0,125 (in black) after being annealed to 500ºC.

The amplitudes can be calculated with the (6) for each film. The film with dc=0,375 has an amplitude of 37.26; Much higher than the amplitude of dc=0,125, of only 1,37.

$$\frac{\Delta\rho_{100-30}}{\rho_{30}} \quad \textbf{(6)}$$

On the other hand, when the films are annealed to 550ºC, the layers with dc=0,125 have a higher amplitude respect dc=0,375, as shown in figure 4.17.

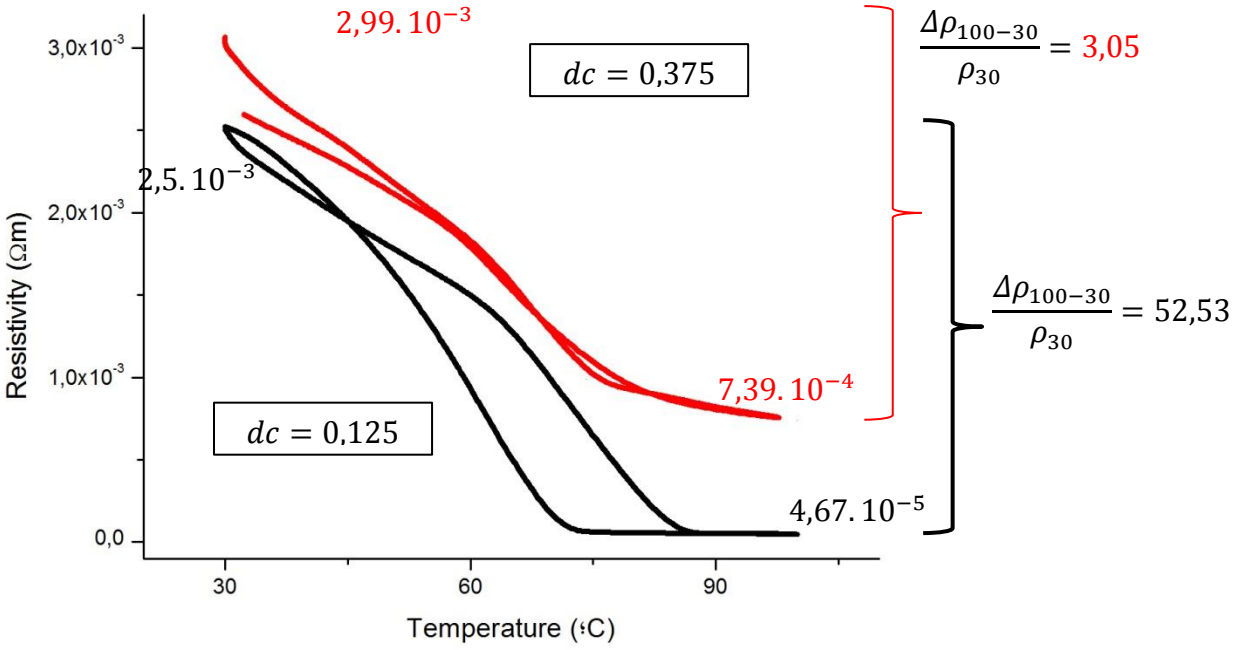

Figure 4.17: Hysteresis loops for dc=0,375 (in red) and for dc=0,125 (in black) after being annealed to 550ºC.

4.5 Gas sensing

After studying all the vanadium oxide films deposited, the most interesting ones for gas sensing applications were tested for ozone detection. Therefore, the films with larger hysteresis loop amplitude and with high resistivity were chosen. The most suitable layers are listed in table 4.2.

Table 4.2: The four most suitable films for gas sensing.

Sample Number	Incidence Angle α (º)	Duty cycle	Annealing temperature (ºC)	Hysteresis loop amplitude
1	85	-	550	5,15
2	85	0,375	500	37,26
3	85	0,375	550	3,05
4	85	0,125	550	52,53

4.5.1 Reactivity test

Firstly, a rough test at room temperature was done to verify that ozone had an impact on the films resistivity. An ozone flow of 1 ppm of concentration was injected on the film during five minutes. An almost immediate reaction could be observed; the resistivity increased with an approximately linear slope (figure 4.18). When the sample was again in dry air, the resistivity took time to stabilize for a value, not necessarily the same as before. Therefore, it is concluded that the vanadium oxide film created does react to ozone but needs a long time to stabilise. It was observed that the films had high sensibility towards humidity too.

Figure 4.18: Resistance vs. time for a five minutes ozone injection on the vanadium oxide thin film with a dc=0,375 and annealed to 500ºC (sample number two).

4.5.2 Repeatability test

After having verified the reactivity of the film, we proceeded to verify if the reactions to ozone were repeatedly equal or followed a pattern. For this reason, ozone was injected during five minutes and then left in dry air for another fifteen minutes (figure 4.19).

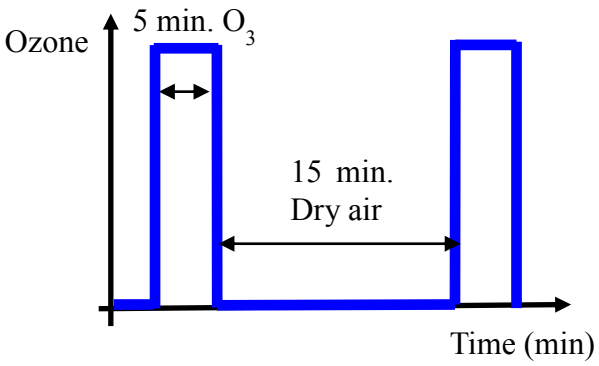

Figure 4.19: Scheme of the cycles of ozone injected.

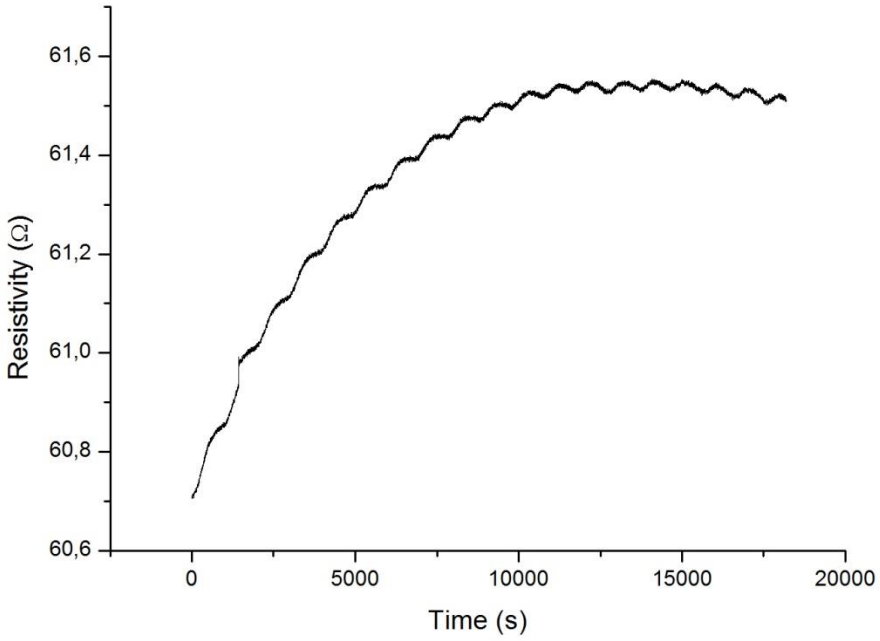

Figure 4.20: Resistivity in front of time for eighteen equal cycles of ozone injection and posterior stabilization.

This operation was repeated for eighteen cycles, obtaining the reactions plotted in figure 4.20. From these results we can conclude that the reaction to ozone becomes each time less meaningful, having a lower slope and, therefore, reactivity (figure 4.21). Heating the sample might make it return to its original values by expulsing the ozone particles attached to the sensor's surface.

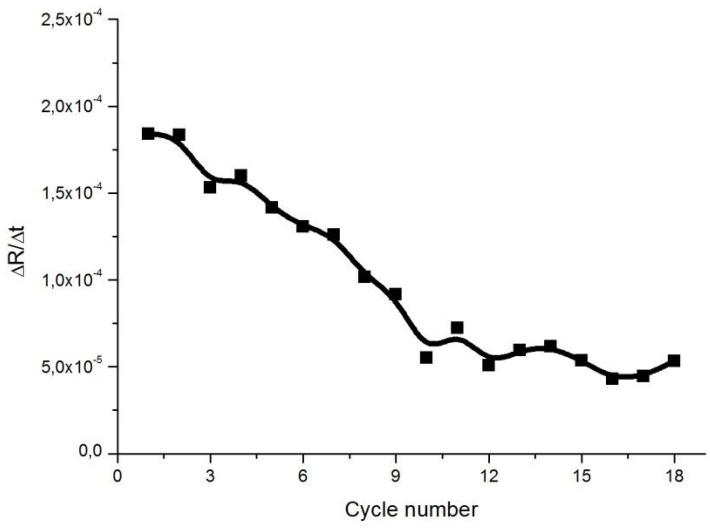

Figure 4.21: Variation of resistivity in front of time for each cycle tested.

4.5.3 Optimal working temperature

It has been proven the reactivity of the film and its capability of being used repeatedly. It is now of great importance to determine correctly the optimal working temperature for our specific sensors. Due to the lack of time to continue with the experiments, a sample had to be chosen to be tested, being it number three; the film with dc=0,375 annealed to 550ºC. It was exposed to two and a half minutes of ozone at a given temperature and then was left to stabilise. Later, it was heated to the next temperature and the process was repeated. Figure 4.22 summarizes the results found.

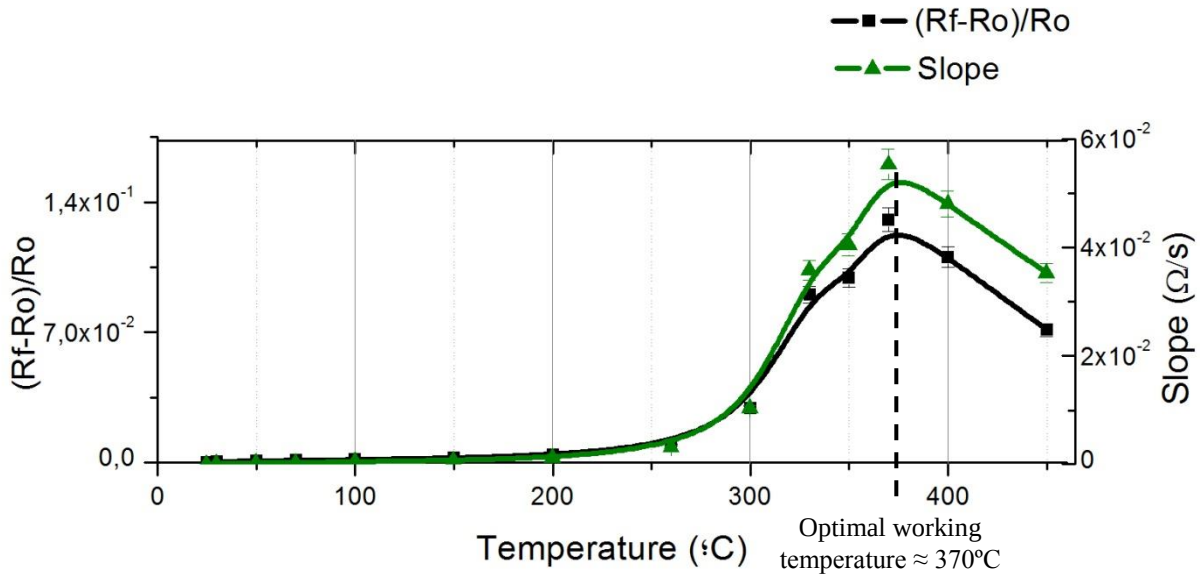

Figure 4.22: Variation of resistivity and slope when injecting ozone for the film with dc=0,375 annealed to 550ºC in function of temperature. The optimal working temperature for this sensor is of approximately 370ºC.

Both the slope of the increase of resistivity when the ozone was injected and the variation of resistivity in front of the initial resistivity are plotted for every temperature studied. The behaviour of these two parameters is alike. It is found that the reactivity increases slightly from room temperature to 300ºC. From 300ºC to approximately 370ºC the reactivity increases sharply, and afterwards decreases.

From these results it can be concluded that the optimal working temperature for the sensor number three is approximately 370ºC. At this temperature the sensor has its strongest reactivity towards ozone and, thus, acts as a better captor.

In comparison to other gas sensors, the optimal temperature found is similar to others such as tin dioxide SnO_2 (380ºC) when detecting hydrogen fluoride [14].

Bibliography of chapter 4

[1] Kusano E, Theil J A and Thornton John A 1663 Deposition of vanadium oxide films by direct-current magnetron reactive sputtering 1988 *J. Vac. Sci. Technol. A* **6**.

[2] Besnard A, Martin N, Sthal F, Carpentier L and Rauch J-Y 2013 Metal-to-Dielectric transition induced by annealing of oriented titanium thin films *Functional Materials Letters* **6(01).**

[3] **[3A]** Besnard A 2010 *Relations nano-structure-conductivité électrique dans des films de chrome architecturés* (Doctoral dissertation) Besançon 31.

[3B] Besnard A 2010 *Relations nano-structure-conductivité électrique dans des films de chrome architecturés* (Doctoral dissertation) Besançon 86.

[3C] Besnard A 2010 *Relations nano-structure-conductivité électrique dans des films de chrome architecturés* (Doctoral dissertation) Besançon 100-101.

[4] Robbie K, Sit J C and Brett M J 1998 Advanced techniques for glancing angle deposition *Journal of Vacuum Science & Technology B* **16(3)** 1115-1122.

[5] Karunasiri R P U, Bruinsma R and Rudnick K 1989 *Phys. Rev. Lett.* **62** 788.

[6] Bales G S and Zangwill A 1989 *Phys. Rev. Lett.* **63** 692.

[7] Turkin A A, Pei Y T, Shaha K P, Chen C Q, Vainshtein D I and De Hosson J T M 2010 On the evolution of film roughness during magnetron sputtering deposition *Journal of Applied Physics* **108(9)** 094330.

[8] Dolatshahi-Pirouz A, Sutherland D S, Foss M and Besenbacher F 2011 Growth characteristics of inclined columns produced by Glancing Angle Deposition (GLAD) and colloidal lithography *Applied Surface Science* **257(6)** 2226-2230.

[9] Lide D R 1991 *CRC handbook of chemistry and physics* CRC press **12**-34.

[10] Schwingenschlogl U and Eyert V 2004 The vanadium Magneli phasesV_nO_{2n-1} *Annalen Der Physik* **13(9)** 475-510.

[11] Pergament A, Stefanovich G and Andreeev V 2013 Comment on "Metal-insulator transition without structural phase transition in V_2O_5 film" [Appl. Phys. Lett. 98, 131907 (2011)] *Applied Physics Letters* **102(17)** 176101.

[12] Kosuge K 1967 The phase diagram and phase transition of the V_2O_3-V_2O_5 system *J. Phys. Chem. Solids* **28** 1613-1621.

[13] Strelcov E, Lilach Y and Kolmakov A 2009 Gas Sensor Based on Metal-Insulator Transition in VO_2 Nanowire Thermistor *Nano Letters* **9(6)** 2322-2326.

[14] Berger F, Sanchez J-B and Heintz O 2009 Detection of hydrogen fluoride using SnO_2-based gas sensors: Understanding of the reactional mechanism *Sensors and Actuators B: Chemical* **143(1)** 152-157.

5. Conclusions and future work

The ultimate goal of this work was to determine the best parameters to create the phase VO_2 in DC magnetron sputtering deposited vanadium films. For the films obtained by the GLAD method, an incidence angle of $\alpha = 85^0$ and an annealing treatment to 550ºC gave the best MIT transition and, thus, had the highest quantity of vanadium dioxide phase.

For the films obtained by GLAD and oxygen pulses, the film with $\alpha = 85^0$, a period of 16 seconds, duty cycle $dc = 0{,}125$ and annealing treatment to 550ºC revealed the best conditions for VO_2 formation.

The aim of creating VO_2 is because of its MIT at around room temperature can be useful for gas captors. Some tests were carried out which verified the reactivity of vanadium dioxide to ozone gas, humidity and temperature. Only one film was able to be tested, being this one the one with dc=0,375annealed to 550ºC. It registered an optimal working temperature of 370 ºC, with a maximum variation of resistivity in front of time of 0,05534 Ω/s.

In conclusion, interesting results never seen before have been carried out for vanadium oxide thin films. For the future, much work can be done to continue this study.

Firstly, the crystallography study enhancing X-ray diffraction (XRD) has to be completed in order to comprehend correctly the MIT transition in VO_2. Secondly, also X-ray photoelectron spectroscopy (XPS) and Raman spectroscopy are needed to verify the chemical composition of the films, in order to state the apparition of vanadium dioxide and its percentage in front of the other vanadium oxides.

Regarding the gas sensing applications, many more tests have to be carried out. Firstly, determine the optimal working temperature for all the other suitable films. Once being determined, vary the exposition to ozone, stabilisation time and humidity to observe the reactions. Also, the

sensors can be tested for other gases such as ammoniac to observe the difference of reaction between exposition to oxidizing or reducing gases.

Finally, plenty of other nano-structures can be created other than inclined columns, zig-zags and spirals. For example, intercalated layers of inclined columns and inclined columns with oxygen pulses can be tested, as in this way we can increase the resistivity of our films, which was found slightly low for gas captors.